Transcription Factor bHLH2 Represses *CYSTEINE PROTEASE77* to Negatively Regulate Nodule Senescence[1][OPEN]

Jie Deng,[a,2] Fugui Zhu,[a,2] Jiaxing Liu,[a] Yafei Zhao,[a] Jiangqi Wen,[b] Tao Wang,[a,3] and Jiangli Dong[a,3,4]

[a]State Key Laboratory of Agrobiotechnology, College of Biological Sciences, China Agricultural University, Beijing 100193, China

[b]Plant Biology Division, Samuel Roberts Noble Research Institute, 2510 Sam Noble Parkway, Ardmore, Oklahoma 73401

ORCID IDs: 0000-0002-4040-1402 (J.De.); 0000-0002-2399-3258 (F.Z.); 0000-0003-3828-7919 (Y.Z.); 0000-0001-5113-7750 (J.W.); 0000-0002-4001-9828 (T.W.); 0000-0003-2643-6358 (J.Do.).

Legume-rhizobia symbiosis is a time-limited process due to the onset of senescence, which results in the degradation of host plant cells and symbiosomes. A number of transcription factors, proteases, and functional genes have been associated with nodule senescence; however, whether other proteases or transcription factors are involved in nodule senescence remains poorly understood. In this study, we identified an early nodule senescence mutant in *Medicago truncatula*, denoted *basic helix-loop-helix transcription factor2* (*bhlh2*), that exhibits decreased nitrogenase activity, acceleration of plant programmed cell death (PCD), and accumulation of reactive oxygen species (ROS). The results suggest that MtbHLH2 plays a negative role in nodule senescence. Nodules of wild-type and *bhlh2*-TALEN mutant plants at 28 d postinoculation were used for transcriptome sequencing. The transcriptome data analysis identified a papain-like Cys protease gene, denoted *MtCP77*, that could serve as a potential target of MtbHLH2. Electrophoretic mobility shift assays and chromatin immunoprecipitation analysis demonstrated that MtbHLH2 directly binds to the promoter of *MtCP77* to inhibit its expression. MtCP77 positively regulates nodule senescence by accelerating plant PCD and ROS accumulation. In addition, the expression of *MtbHLH2* in the nodules gradually decreased from the meristematic zone to the nitrogen fixation zone, whereas the expression of *MtCP77* showed enhancement. These results indicate that MtbHLH2 and MtCP77 have opposite functions in the regulation of nodule senescence. These results reveal significant roles for MtbHLH2 and MtCP77 in plant PCD, ROS accumulation, and nodule senescence, and improve our understanding of the regulation of the nodule senescence process.

Legumes play an important role in sustainable agriculture by increasing crop yields due to their symbiotic association with rhizobia (Fox et al., 2007). Symbiotic nitrogen fixation occurs in special organs, named nodules, and these organs provide a suitable microenvironment for supplying the carbon obtained from photosynthesis to rhizobia. Rhizobia can fix nitrogen by nitrogenase to provide ammonium to legumes (Stonoha-Arther and Wang, 2018). The late stage in the development of nodules, including determinate and indeterminate nodules, regulates their fate, namely senescence. Determinate nodules have nonpersistent meristems and result from the development of radial gradients, as has been observed in *Glycine max*, *Lotus japonicus*, *Phaseolus vulgaris*, and *Vigna unguiculata*. The senescence of determinate nodules begins at the nodule center and gradually extends to the periphery (Puppo et al., 2005). Indeterminate nodules, such as those in *Medicago truncatula*, *Pisum sativum*, *Vicia faba*, and *Trifolium repens*, contain five different zones: zone I (meristematic zone), zone II (infection zone), zone III (nitrogen fixation zone), zone IV (senescence zone), and zone V. Zone IV does not exist during the early stages of nodule differentiation but appears with nodule development. In addition, zone IV increases in size with increased age of the host plant and triggers the degradation of symbiosomes in response to aging or environmental stress. Zone V is proximal to zone IV and shows ultra-structural features of free-living bacteria

[1]This work was financially supported by grants from the National Natural Science Foundation of China (31772658 and 31571587) and the Project for Extramural Scientists of the State Key Laboratory of Agrobiotechnology (2018SKLAB6-22).

[2]These authors contributed equally to the article.

[3]Senior authors.

[4]Author for contact: dongjl@cau.edu.cn.

The author responsible for distribution of materials integral to the findings presented in this article in accordance with the policy described in the Instructions for Authors (www.plantphysiol.org) is: Jiangli Dong (dongjl@cau.edu.cn).

J.De. and F.Z. performed most of the experiments, collected the data, and wrote the article; J.L. analyzed the data; Y.Z. participated in the construction of some vectors; J.W. provided the *Tnt1*-insertion mutant lines; J.Do. and T.W. conceived the project, designed the experiments, and revised the article; all of the authors read and approved the final article.

[OPEN]Articles can be viewed without a subscription.

www.plantphysiol.org/cgi/doi/10.1104/pp.19.00574

(Timmers et al., 2000; Dupont et al., 2012). During nodule senescence, the color of the nitrogen fixation zone is converted from pink, which is associated with functional leghemoglobin, to green, which is related to nitration of the heme group of leghemoglobin (Navascués et al., 2012). At the ultrastructural level, the following changes in cell organelles and symbiosomes have been observed: the electron density of the cytoplasm becomes progressively lower, the loose plasma membrane separates from the cell wall, the cell wall becomes damaged, bacteroids undergo lysis, and the peribacteroid membrane is degraded (Timmers et al., 2000; Van de Velde et al., 2006). Another study reported the existence of a conical front in the senescence zone of indeterminate nodules (Pérez Guerra et al., 2010). The early signs of senescence occur in some infected cells in the center of the nitrogen fixation zone and then gradually extended to the proximal cell layers of the nodule periphery, leading to the formation of a conical front during nodule growth (Pérez Guerra et al., 2010).

At the senescence stage, several kinases, nodule-specific Cys-rich (NCR) peptides, membrane proteins, and other functional genes in *L. japonicus* or *M. truncatula* are involved in nodule senescence. *MtSymCRK* encodes a Cys-rich receptor-like kinase of the non-Arg Asp (nonRD) family and is required to prevent nodule senescence and to avoid defense-like reactions (Berrabah et al., 2014). *DEFECTIVE NITROGEN FIXATION7* (*MtDNF7*) encodes NCR169, which contributes to bacteroid differentiation and is associated with early senescence of the symbiotic cells (Horváth et al., 2015). Two mutants of *MtNCR211*, *early senescent nodule1* (*esn1*) and *dnf4*, both present spherically shaped nodules, ineffective nitrogen fixation, and premature senescence (Xi et al., 2013; Kim et al., 2015). *NITROGEN FIXATION SPECIFICITY1* (*MtNFS1*) and *MtNFS2* encode NCR peptides and negatively regulate nitrogen fixation symbiosis in a rhizobial strain-specific manner (Wang et al., 2017; Yang et al., 2017; Wang et al., 2018). SYMBIOTIC SULFATE TRANSPORTER1 (LjSST1) is a nodule-specific sulfate transporter that is localized on the symbiosome membrane (Krusell et al., 2005). *INEFFECTIVE GREENISH NODULES1* (*LjIGN1*) encodes an ankyrin-repeat membrane protein that is essential for the differentiation or persistence of bacteroids and symbiosomes (Kumagai et al., 2007). *STATIONARY ENDOSYMBIONT NODULE1* (*LjSEN1*) is an integral membrane protein required for nitrogen fixation activity and the differentiation of bacteroids or symbiosomes (Hakoyama et al., 2012). *REGULATOR OF SYMBIOSOME DIFFERENTIATION* (*MtRSD*) encodes a Cys-2/histone-2 (C_2H_2) transcription factor that inhibits the expression of *VESICLE-ASSOCIATED MEMBRANE PROTEIN721A* (*MtVAMP721a*), which indicates that it influences nitrogen fixation and the differentiation of symbiosomes and bacteroids (Sinharoy et al., 2013). NODULES WITH ACTIVATED DEFENSE1 (MtNAD1) is a small uncharacterized protein localized in the endoplasmic reticulum, which indicates that it plays a positive role in the maintenance of rhizobial endosymbiosis (Wang et al., 2016; Domonkos et al., 2017). MtDNF2 encodes a phosphatidylinositol-specific phospholipase C X domain (PI-PLC-XD) protein, and its mutants exhibit fewer cell layers in the infection zone, where bacteria do not differentiate, and rapid senescence (Bourcy et al., 2013). ASPARTIC PEPTIDASE NODULE-INDUCED1 (LjAPN1) is a nepenthesin-type aspartic peptidase that plays a necessary role in nitrogen fixation symbiosis in a rhizobial strain-dependent manner (Yamaya-Ito et al., 2018). *M. truncatula* has five nodule-specific PLAT (polycystin-1, lipoxygenase, alpha toxin) domain proteins (NPDs), and lines with different mutation combinations presented smaller nodules, earlier nodule senescence, or ineffective nodules (Trujillo et al., 2019).

In addition to various mutations in symbiotic genes, nodule senescence is also affected by diverse environmental stresses, such as drought, salt, cold, continuous darkness, and nitrate (Dupont et al., 2012), and previous studies have indicated that different stresses accelerate nodule senescence (Pérez Guerra et al., 2010; Dhanushkodi et al., 2018). Moreover, phytohormones, such as abscisic acid, ethylene, and jasmonic acid (JA), might positively regulate nodule senescence (Puppo et al., 2005; Van de Velde et al., 2006; Karmarkar, 2014; Guinel, 2015). The positive role of abscisic acid induces nodule senescence (González et al., 2001; Puppo et al., 2005) and the expression of some senescence-associated genes (SAGs; Fukudome et al., 2019). The positive roles of ethylene and JA have been suggested by the induction of *ETHYLENE RESPONSE FACTOR* (*ERF*) transcription factors and genes related to ethylene and JA biosynthesis (Van de Velde et al., 2006; Serova et al., 2017). Ethylene can also trigger plant defense responses and results in necrosis that colocalizes with infected cells by rhizobia (Berrabah et al., 2018). GAs play a negative role in nodule senescence (Van de Velde et al., 2006; Hayashi et al., 2014; Serova et al., 2019), and nitric oxide positively regulates nodule senescence (Cam et al., 2012; Berger et al., 2019).

A pivotal characteristic of the nodule senescence process is the involvement of proteolytic activity, which can act in the degradation of misfolded or modified proteins (Pladys and Vance, 1993). Cys protease (CP; EC3.4.22) uses catalytic Cys as a nucleophile during proteolysis (van der Hoorn, 2008). Most plant Cys proteases belong to the papain (C1) and legumain (C13) families, and metacaspases (family C14) and calpains (family C2, calcium-dependent proteases) have been detected in plants (Grudkowska and Zagdańska, 2004). The plant papain-like Cys proteases (PLCPs) are the most researched of all Cys proteases. PLCP genes are significantly induced in senescent nodules of *G. max*, *Astragalus sinicus*, *P. sativum*, and *M. truncatula* (Fedorova et al., 2002), such as *GmCYSP1* (Alesandrini et al., 2003; Oh et al., 2004), *AsNodf32* (Naito et al., 2000), *PsCYP1*, and *PsCYP15A* (Kardailsky and Brewin, 1996; Vincent and Brewin, 2000). *MsCYP15A*, *AsNodf32*, and

MtCP6 belong to the PLCP family and positively regulate nodule senescence (Sheokand et al., 2005; Li et al., 2008; Pierre et al., 2014). The senescence of root nodules is modulated by transcription factors. To date, three transcription factors, namely *MtATB2*, *MtNAC969*, and *MtNAC920*, have been found to be involved in nodule senescence. *MtATB2*, which encodes a bZIP transcription factor, is more highly expressed in senescent nodules (D'haeseleer et al., 2010). The knockdown of *MtNAC969* results in a higher number of amyloplasts in the nitrogen fixation zone and thereby triggers premature senescence (de Zélicourt et al., 2012). *MtNAC920*, which is induced by nitrate and ethylene, serves as a positive regulator of nodule senescence and directly targets *MtCP2*, which was previously reported to be a marker gene for nodule senescence (Karmarkar, 2014). However, whether other proteases or transcription factors are involved in nodule senescence remains unclear.

In this study, we demonstrate that a basic helix-loop-helix (bHLH) transcription factor in *M. truncatula*, named MtbHLH2, is a key regulatory component that negatively regulates nodule senescence. Moreover, we show that MtbHLH2 binds to the promoter of the Cys protease *MtCP77* to repress its expression and reveal that MtCP77 plays a positive role in nodule senescence.

RESULTS

MtbHLH2 Is a Negative Regulator of Nodule Senescence

The *M. truncatula* mutant line NF11035 with early nodule senescence (Fig. 1D) was isolated from the *M. truncatula Tnt1* insertion mutant database by forward genetic screening. To identify which gene was involved in nodule senescence, 16 flanking sequence tags (FSTs) available in the *M. truncatula* Mutant Database at the Noble foundation for this mutant line were analyzed. Only one *Tnt1* FST inserted between 1916 and 1917 bp of *Medtr5g030430* was linked to the phenotype, and this gene was denoted *basic helix-loop-helix transcription factor2* (*MtbHLH2*; Fig. 1, A and B). We then selected another *Tnt1* insertion mutant (NF13601) of *MtbHLH2*, in which the *Tnt1* FST was located between 1022 and 1023 bp of *MtbHLH2* (Fig. 1, A and B). The phenotype of NF13601 was consistent with that of NF11035 and was associated with prematurely senescent nodules (Fig. 1D). The *MtbHLH2* full-length transcripts in NF11035 and NF13601 were not detected by RT-PCR, which suggested that the expression of *MtbHLH2* was impaired (Fig. 1C).

To elucidate the influences of the *MtbHLH2* mutation on nodule senescence, the nodules of the wild-type and *bhlh2* mutant were harvested at 28 d postinoculation (dpi), sectioned, stained with toluidine blue, and observed. Compared with the pattern observed in the wild type, most of the senescence zone and a small part of the nitrogen fixation zone were found in the *bhlh2* nodules (Fig. 1E). To investigate the effects of the *MtbHLH2* mutation at the ultrastructural level, the nitrogen fixation zone of the wild type and *bhlh2* nodules was observed at 28 dpi with a transmission electron microscope (TEM). In agreement with the light microscopy observations, the nitrogen fixation zone was substantially modified in the *bhlh2* mutants. In the wild-type nodules, symbiosomes completely filled the infected cells, whereas in the mutant nodules, symbiosomes appeared to be loosely placed within the infected cells, the host cells died, and the symbiosomes decayed (Fig. 1F). This result suggested that the mutation of *MtbHLH2* might promote host cell death and symbiosome decay. The nitrogenase activity of the wild type and *bhlh2* mutant nodules at 28 dpi was measured through an acetylene reduction assay (ARA). The nitrogenase activity of the *bhlh2* mutants was significantly lower than that of the wild type, which suggested that MtbHLH2 affects the efficiency of symbiotic nitrogen fixation (Fig. 1G).

To further determine the function of *MtbHLH2* in nodule senescence, *MtbHLH2*-knockout mutants were obtained using transcription activator-like effector nuclease (TALEN) technology. Stable transgenic lines were generated by *Agrobacterium tumefaciens*-mediated transformation and identified by sequencing. The *bhlh2*-T36- and *bhlh2*-T43-knockout mutants containing 58- and 47-bp deletions, respectively, triggered the frameshift mutation (Fig. 2A). The *bhlh2*-T138-knockout mutant caused the deletion of a large fragment, which included the transcriptional start site (ATG; Fig. 2A). The phenotype of the *bhlh2*-TALEN mutants was similar to that of the *Tnt1*-insertion mutants (Fig. 2, B–D), which further confirmed that the MtbHLH2 single-gene mutation affected nodule senescence.

MtbHLH2 Is Localized in the Nucleus and Encodes a Transcriptional Repressor

The cDNA fragment of *MtbHLH2* was 2034 bp in length, and this gene did not contain introns (Fig. 1A). This transcript was predicted to encode a 677-amino-acid protein (Supplemental Fig. S1A). The typical bHLH motif was located in the C terminus of MtbHLH2, in which the basic region contained five basic amino acids for DNA binding and highly conserved hydrophobic residues in helices 1 and 2 for protein-protein interactions (Fig. 3A). The phylogenetic analysis showed that MtbHLH2 belongs to subfamily III (d+e; Supplemental Fig. S1B; Supplemental Notes S1). These results suggest that MtbHLH2 could be a functional transcription factor.

To address the subcellular localization of MtbHLH2, MtbHLH2-eGFP was transiently expressed in onion (*Allium cepa*) epidermal cells. Costaining with 4′,6-diamidino-2-phenylindole (DAPI), a dye that is used for nuclear quantitation, showed that MtbHLH2 was localized in the nucleus (Fig. 3B) with an intensity correlation quotient (ICQ) of 0.386 (Supplemental Fig. S2). A protein immunoblot analysis confirmed that MtbHLH2 was detected only in the nucleus (Fig. 3C), which is

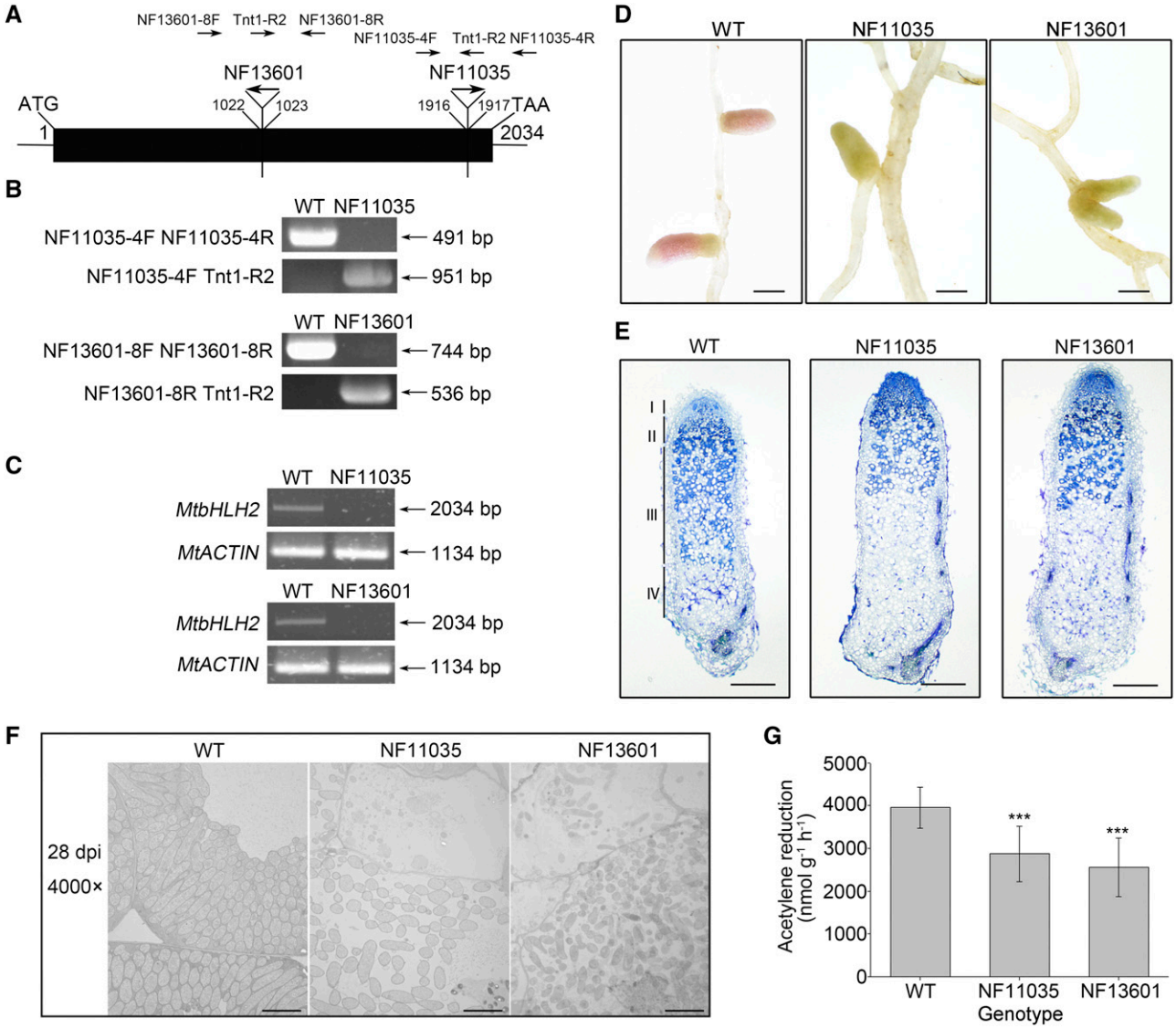

Figure 1. The mutation of *MtbHLH2* results in early-nodule senescence and decreased nitrogen fixation. A, Schematic diagram of the *Tnt1* insertion site in the *MtbHLH2* gene. The box shows the exon, and this gene has no intron. The orientations of *Tnt1* are indicated. B, Identification of homozygous lines of *Tnt1*-insertion mutants (NF11035 and NF13601). The insertion site analysis was performed at the DNA level. C, RT-PCR analysis of *MtbHLH2* transcripts in the wild type (WT) and *bhlh2 Tnt1*-insertion mutants. *MtACTIN* was used as the loading control. D, Light micrographs of wild-type and *bhlh2 Tnt1*-insertion mutant nodules at 28 dpi. Bars = 1 mm. E, Longitudinal sections of toluidine blue-stained wild-type and *bhlh2 Tnt1*-insertion mutant nodules at 28 dpi. The section thickness is 8 μm. The different zones of the nodules (I–IV) are shown. I, Meristematic zone; II, infection zone; III, nitrogen fixation zone; IV, senescence zone. Bars = 200 μm. F, Electron micrographs of longitudinal ultrathin sections of wild-type and *bhlh2 Tnt1*-insertion mutant nodule cells from the nitrogen fixation zone at 28 dpi (4000× magnification). Bars = 5 μm. G, The nitrogenase activity of wild type and *bhlh2 Tnt1*-insertion mutant nodules (NF11035 and NF13601) at 28 dpi was determined by an ARA. The error bars represent the ± SD of the means, and asterisks indicate a significant difference between the wild-type and *bhlh2 Tnt1*-insertion mutant nodules (one-way ANOVA followed by Tukey's post-hoc test, $***P < 0.001$, $n = 19$). Similar results were obtained from three independent experiments.

consistent with the fluorescence data. These findings verified that MtbHLH2 was localized to the nucleus.

To test whether MtbHLH2 serves as a transcriptional activator or repressor, a transient expression assay was performed using yeast cells with the GAL4 DNA-binding domain (DBD) reporter system. Only the positive control grew well on synthetic dropout minimal base medium lacking Trp, His, and adenine and displayed X-α-gal activity. The DBD-MtbHLH2 and negative control did not grow (Fig. 3D), which implied that MtbHLH2 did not act as a transcriptional activator in yeast. The reporter construct 35S-UAS-GUS (Tao et al., 2013) was then cotransformed with G4DBD or G4DBD-MtbHLH2 into *Nicotiana benthamiana* leaves. Strong

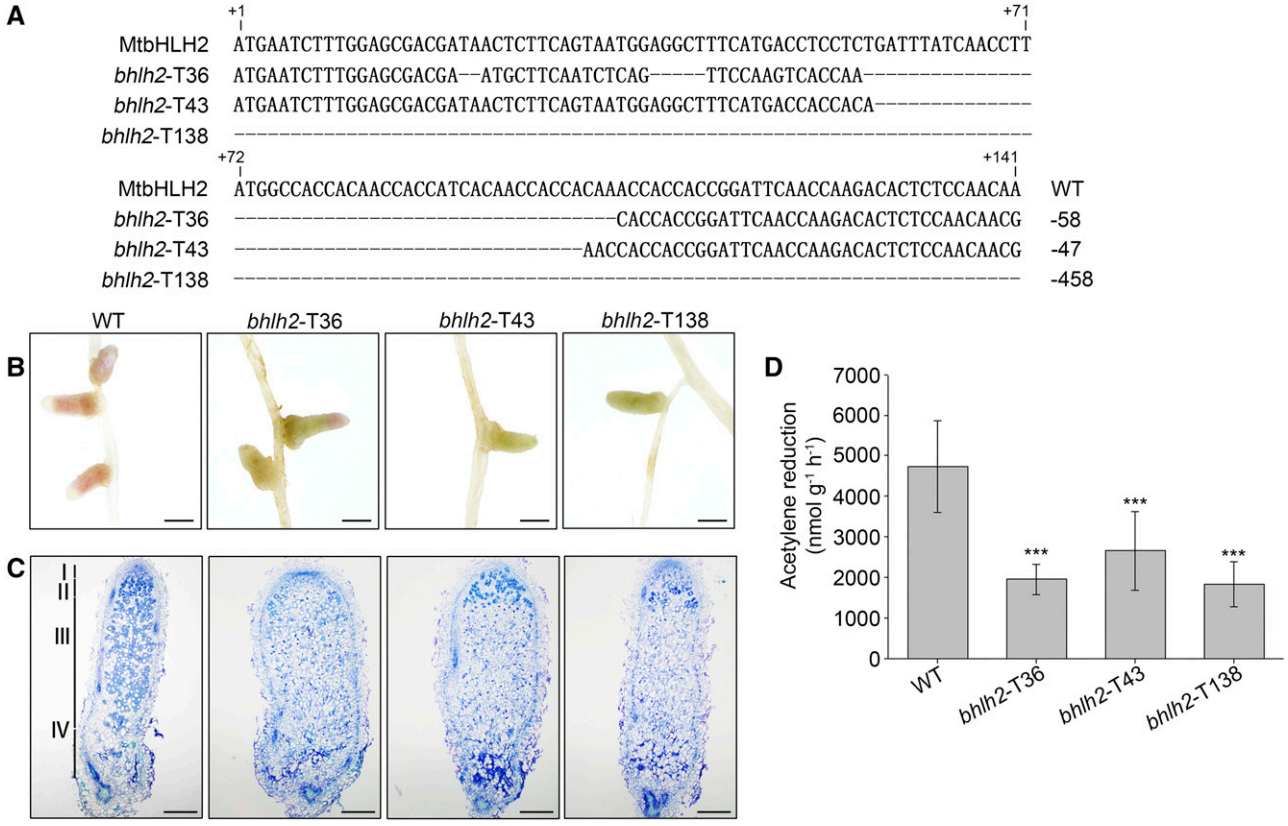

Figure 2. Identification and phenotype of the *bhlh2*-TALEN mutant nodules. A, The *bhlh2*-TALEN mutants *bhlh2*-T36, *bhlh2*-T43, and *bhlh2*-T138 mutants had deletions of 58, 47, and 458 bp, respectively. The first base of the transcriptional start site (ATG) is shown at position +1. B, Light micrographs of wild-type (WT) and *bhlh2*-TALEN mutant nodules at 28 dpi. Bars = 1 mm. C, Longitudinal sections of toluidine blue-stained wild-type and *bhlh2*-TALEN mutant nodules at 28 dpi. The section thickness is 8 μm. The different zones of the nodules (I–IV) are shown. I, Meristematic zone; II, infection zone; III, nitrogen fixation zone; IV, senescence zone. Bars = 200 μm. D, The nitrogenase activity of wild-type and *bhlh2*-TALEN mutant nodules at 28 dpi was determined by an ARA. The error bars represent the ± SD of the means, and asterisks indicate a significant difference between the wild-type and *bhlh2*-TALEN mutant nodules (one-way ANOVA followed by Tukey's post-hoc test, ***$P < 0.001$, $n = 19$). Similar results were obtained from three independent experiments.

GUS staining was obtained with the combination of 35S-UAS-GUS with G4DBD, whereas considerably weakened GUS staining was obtained with the combination of 35S-UAS-GUS with G4DBD-MtbHLH2 in *N. benthamiana* leaves (Fig. 3E). Transient GUS quantitative experiments were performed, and the results revealed that MtbHLH2 significantly repressed the expression of *GUS*. These results demonstrated that MtbHLH2 was a transcriptional repressor.

To determine the tissue expression pattern of *MtbHLH2*, the transcript level of *MtbHLH2* in different tissues of *M. truncatula* R108 at 28 dpi with *Sinorhizobium meliloti* 1021 (Sm1021) was analyzed by RT-qPCR, and *MtACTIN* (*Medtr3g095530*) was selected as the reference gene because the expression of *MtACTIN* was found to be stable at the lowest *M* value ($M = 0.047 < 0.5$). The results showed that *MtbHLH2* was expressed in the roots, stems, leaves, and nodules (Fig. 4A). The expression of *MtbHLH2* during nodule organogenesis was also analyzed, and the RT-qPCR results indicated that the expression of *MtbHLH2* first showed a slow decrease until the lowest point was reached at 28 dpi and then exhibited a slow increase (Fig. 4B). These results were consistent with the data of the *M. truncatula* Gene Expression Atlas (Supplemental Fig. S3A). The putative promoter-GUS-transgenic lines were obtained from *M. truncatula* by *A. tumefaciens*-mediated transformation, and a histochemical analysis of GUS staining in stable transgenic lines was performed at 14, 28, and 42 dpi with Sm1021. The results indicated that *MtbHLH2* was expressed in the vascular bundles of roots, stems and nodules as well as in leaf veins (Fig. 4, C–H). The expression of *MtbHLH2* decreased gradually from the meristematic zone to the nitrogen fixation zone (Fig. 4, I–K), and this expression pattern was consistent with the data in the Symbimics website (https://iant.toulouse.inra.fr/symbimics; Roux et al., 2014; Supplemental Fig. S3B). To gain insight into the relationship between the *MtbHLH2* expression pattern in nodules and its negative regulation of nodule senescence, we performed high-throughput RNA-sequencing (RNA-seq) studies.

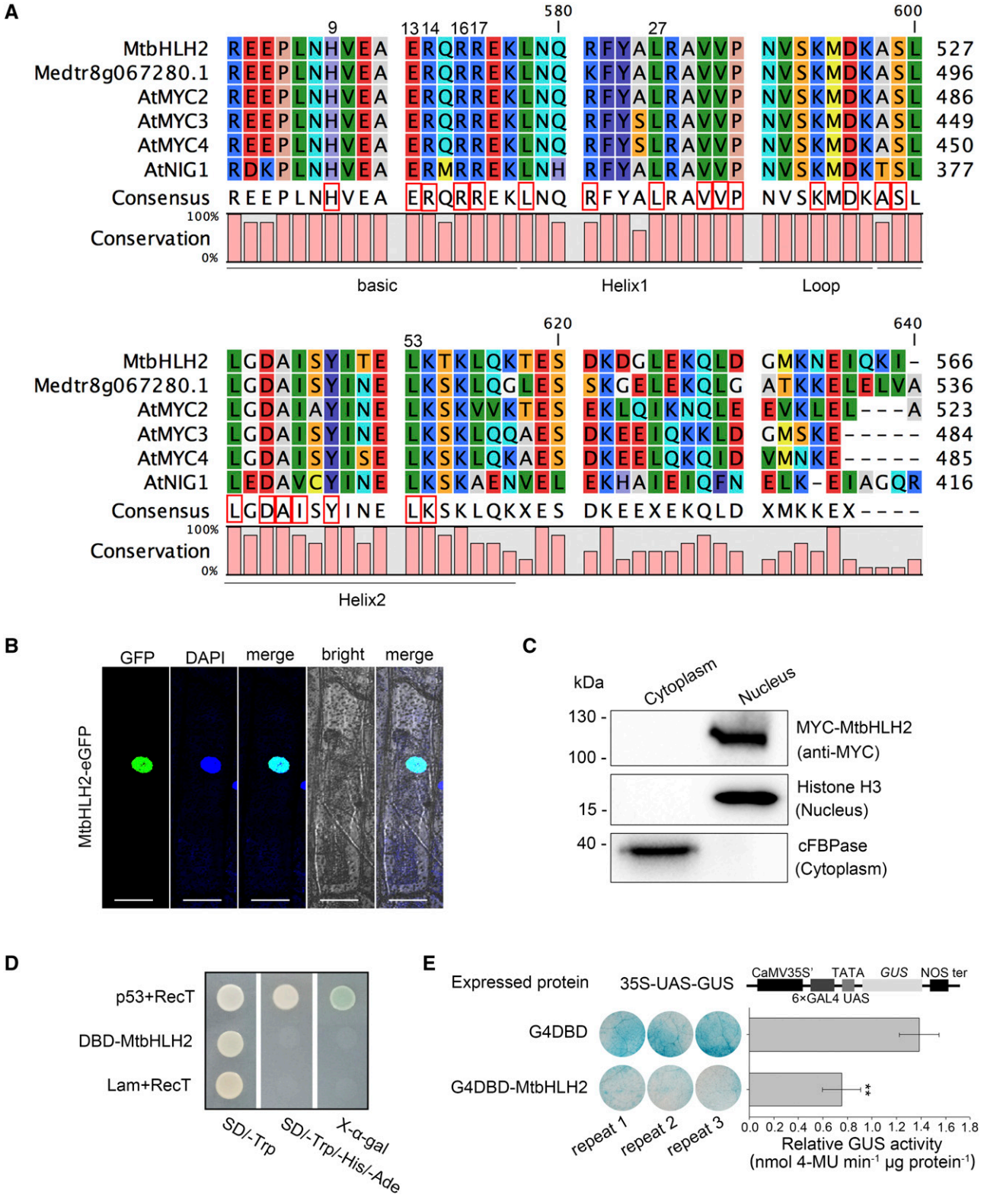

Figure 3. MtbHLH2 is localized in the nucleus and serves as a transcriptional repressor. A, bHLH domain structures of some III (d+e) subfamily members in *M. truncatula* and Arabidopsis. These III (d+e) subfamily sequence alignments were constructed using CLC Sequence Viewer 7.0 software. The conserved residues for DNA binding or protein-protein interaction are shown by red boxes. B, Subcellular localization of MtbHLH2 in onion epidermal cells. The MtbHLH2-eGFP fusion protein driven by the Cauliflower mosaic virus (CaMV) 35S promoter was transiently expressed in onion epidermal cells via particle bombardment. The

Transcriptome Analysis of the Wild-Type and *bhlh2*-TALEN Mutant Nodules

Because the *Tnt1* mutants contained many insertion sites, *MtbHLH2*-TALEN mutants were subjected to transcriptome sequencing. To investigate the target genes and pathways regulated by MtbHLH2, RNA-seq digital gene expression profiling was performed using wild-type and *bhlh2*-T36 nodules at 28 dpi. The total number of clean reads in the wild-type and *bhlh2*-T36 nodules was 72,311,379 and 77,666,037, respectively. Among the 929 differentially expressed genes, 433 and 496 genes were upregulated and downregulated ($|\log_2\text{fold change}| \geq 0.6$, $P \leq 0.05$) in the *bhlh2*-T36 nodules compared with the wild-type nodules, respectively. The enrichment of Kyoto Encyclopedia of Genes and Genomes (KEGG) pathways showed that the upregulated genes were related to purine and pyrimidine metabolism, vitamin B_6 metabolism, starch and Suc metabolism, and diterpenoid biosynthesis (Supplemental Fig. S4A). The enrichment of KEGG pathways revealed that the downregulated genes were involved in starch and Suc metabolism and the degradation of various branched amino acids, glycosaminoglycan, and amino sugar (Supplemental Fig. S4B). The analysis of the Gene Ontology (GO) terms of the differentially expressed genes showed that these genes were associated with carbohydrate biosynthetic process in the biological process category and in the transfer of hexosyl groups, the transfer of glycosyl groups, and Cys-type endopeptidase activity in the molecular function category (Fig. 5A).

Due to the transcriptional repression activity of MtbHLH2, we subsequently focused on upregulated genes. These genes included *MtDMPP950* and *MtDMPP910*, which influence the homeostasis of the active form of coenzyme vitamin B_6 (ShuoHao et al., 2019); *MtKAO230* and *MtKAO240*, which are associated with GA biosynthesis (Sun, 2008); *MtGPA*, which promotes the production of ADP-Glc, the precursor of amylose (Hädrich et al., 2012); *MtFRUCT2*, which is related to Suc degradation and might be involved in leaf senescence (Buchanan-Wollaston et al., 2005; Gómez et al., 2006); *MtCaspase*, which is involved in programmed cell death (PCD) and the hypersensitive response (Coll et al., 2011); and senescence-associated genes (Lohman et al., 1994; Zhang et al., 2012b), such as Cys protease and PP2C-type protein phosphatase. To examine whether these genes were modulated by MtbHLH2, the relative expression of these candidate genes was detected by reverse transcription quantitative PCR (RT-qPCR). The findings revealed that the genes were upregulated in the *bhlh2* mutant nodules at 28 dpi compared with those in the wild-type nodules, and the most highly upregulated gene was a *PLCP* involved in Cys-type endopeptidase activity, which is denoted *MtCP77* (Fig. 5B; Supplemental Table S1). The results indicated that MtbHLH2 might negatively regulate the expression of candidate genes that respond to the nodule senescence process.

MtbHLH2 Directly Binds to the Promoter of *MtCP77* In Vitro and In Vivo

An EMSA was performed to determine whether MtbHLH2 can bind to the promoter of *MtCP77*. Both probes contained three G-boxes in the *MtCP77* promoter (Fig. 6A). The MtbHLH2 protein can bind to both wild-type probes (P1 and P2), and this binding effectively competed with the respective unlabeled probe. MtbHLH2 did not bind to the respective mutant probe (the 5′-AAAAAA-3′ motif instead of the 5′-CACGTG-3′ motif), and neither unlabeled mutant probe competed with the binding of MtbHLH2 to the wild-type probe (Fig. 6B). These results demonstrated that MtbHLH2 could bind to G-box cis-elements in the promoter region of *MtCP77* in vitro.

Because MtbHLH2 could bind to the promoter of *MtCP77* in vitro, whether MtbHLH2 could also bind to the promoter of *MtCP77* in vivo was then investigated. A chromatin immunoprecipitation (ChIP) experiment was performed using empty vector (EV)-transgenic lines and *MtbHLH2*-FLAG (*MtbHLH2*OE)-transgenic lines (Supplemental Fig. S5). The anti-FLAG antibody was used for immunoprecipitation. In the nodules and roots collected from the materials at 28 dpi, the *MtCP77* promoter fragment F2R2 (primers MtCP77-ChIP-qF2 and MtCP77-ChIP-qR2) containing the G-box cis-element was enriched in *MtbHLH2*-FLAG-transgenic lines compared with the EV-transgenic lines used as a control, whereas promoter fragments lacking the G-box

Figure 3. (*Continued.*)
fluorescence signals, namely GFP and DAPI, were detected by a confocal laser scanning microscope (CLSM) using excitation wavelengths of 488 and 385 nm, respectively. Bars = 50 μm. C, Cellular fractionation and immunoblot analysis of transiently expressed MYC-MtbHLH2 in *N. benthamiana* leaves. Anti-histone H3 and anti-cFBPase were used as nucleus and cytoplasm markers, respectively. D, MtbHLH2 has no transcriptional activation activity in yeast. The GAL4 DBD-MtbHLH2 construct was transformed into the yeast strain AH109. The transformed yeast solutions were spotted in SD medium lacking Trp, His, and adenine. The plates were incubated for 3 d and examined through an X-α-gal assay. p53+RecT (positive control); Lam+RecT (negative control). E, MtbHLH2 is a transcriptional repressor. The transcriptional activity of MtbHLH2 in *N. benthamiana* leaves was detected using a GAL4/UAS-based system. CaMV 35S′, 35S promoter without a TATA box; 6×GAL4 UAS, six copies of the GAL4-binding site (UAS); NOS ter, terminator of the nopaline synthase gene; G4DBD, GAL4 DNA-binding domain; G4DBD-MtbHLH2, G4DBD fused with MtbHLH2. Measurements obtained through transient GUS activity assays are shown on the right. The error bars represent the ± SD of the means, and asterisks indicate a significant difference between G4DBD and G4DBD-MtbHLH2 (Student's *t* test, $^{**}P < 0.01$, $n = 3$).

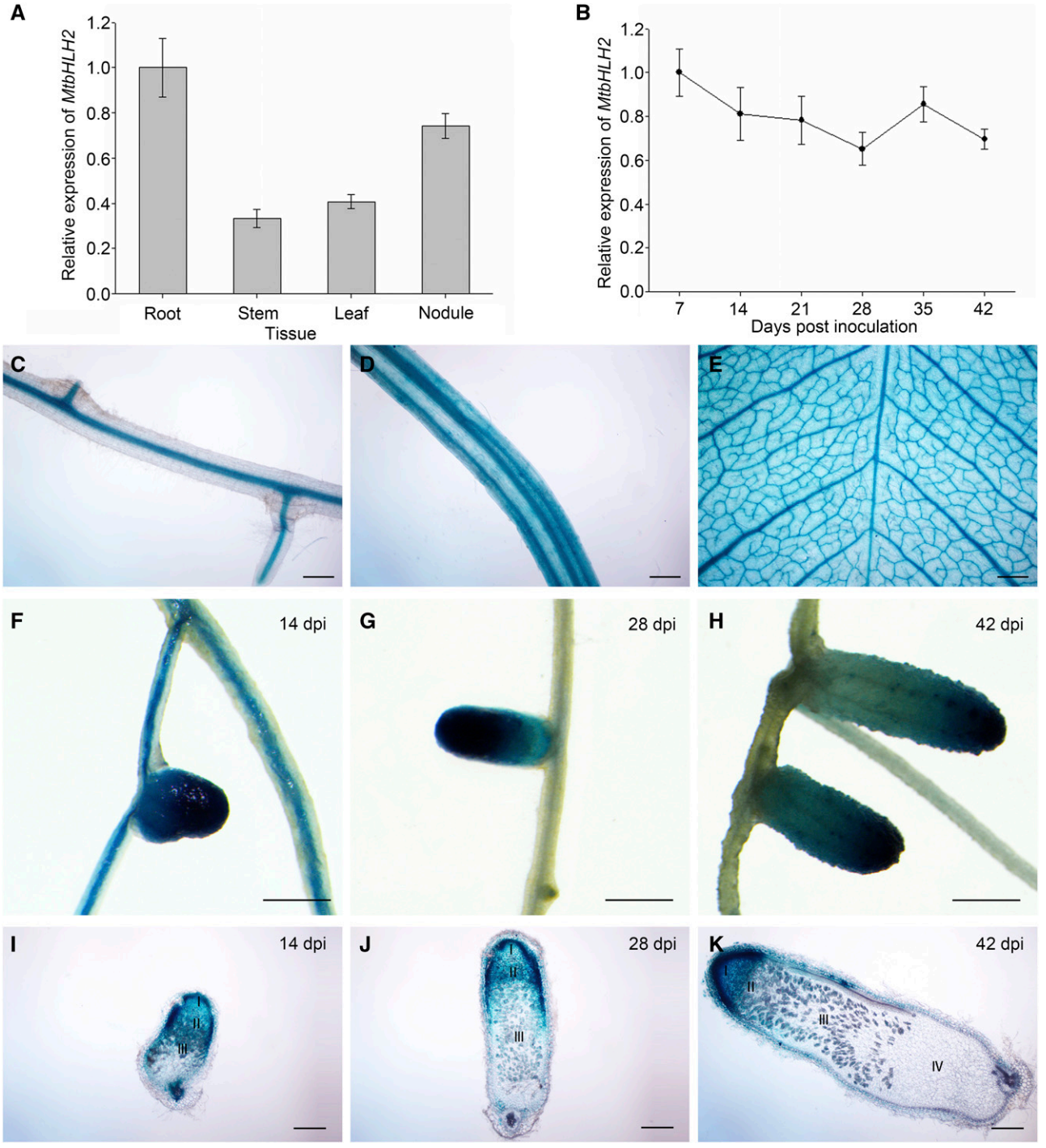

Figure 4. Expression pattern of *MtbHLH2*. A, The relative expression of *MtbHLH2* in the roots, stems, leaves, and nodules of wild-type plants at 28 dpi with *Sinorhizobium meliloti* 1021 was measured by RT-qPCR using *MtACTIN* as the reference gene. The error bars represent the ± SD of the means of two biological replicates. B, Relative expression of *MtbHLH2* in the nodules of wild-type plants at different time points after inoculation (7, 14, 21, 28, 35, and 42 dpi) with *S. meliloti* 1021. *MtACTIN* was used as the reference gene. The error bars represent the ± SD of the means of two biological replicates. C to K, GUS staining of *MtbHLH2* expressed in *M. truncatula*. The expression pattern of the 2.3-kb promoter region of *MtbHLH2* was detected. Expression of *MtbHLH2* in the roots (C), stems (D), and leaves (E) at 14 dpi with *S. meliloti* 1021. F to H, GUS staining of nodules on stable transgenic plants at 14 (F), 28 (G), and 42 dpi (H). I to K, Sections of nodules at 14 (I), 28 (J), and 42 dpi (K). The section thickness is 80 μm. The different zones of the nodules (I–IV) are shown. I, Meristematic zone; II, infection zone; III, nitrogen fixation zone; IV, senescence zone. Bars = 200 μm (C–E and I–K) and 1 mm (F–H).

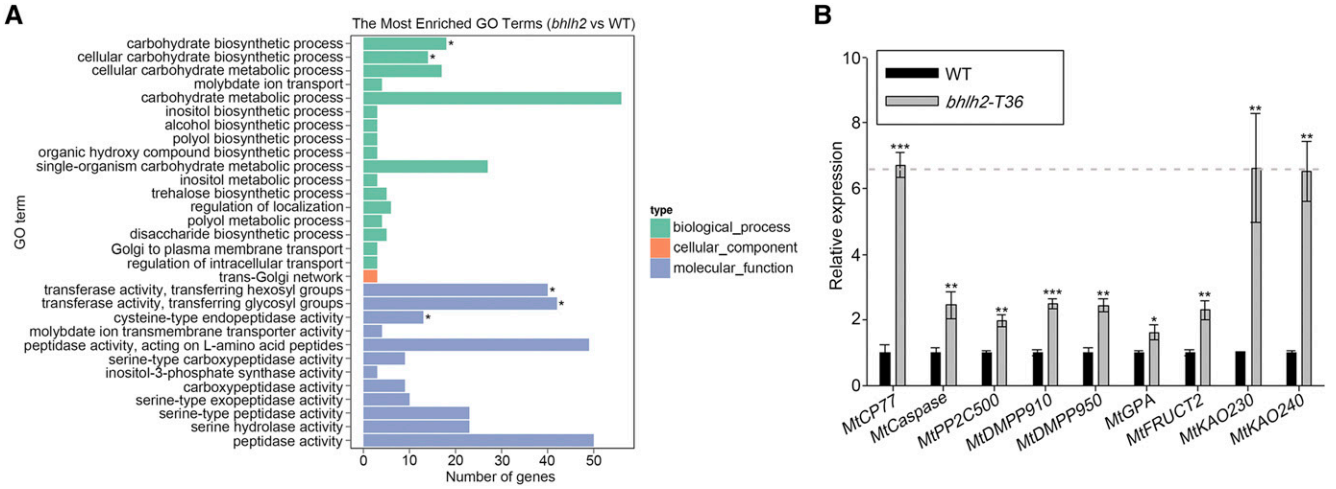

Figure 5. MtbHLH2 regulates various genes involved in nodule senescence. A, GO analysis of differentially expressed genes at the biological process, cellular component, and molecular function levels. The 30 most significantly enriched GO terms were analyzed using the GOseq R package. GO terms with an adjusted $P < 0.05$ were considered significantly enriched. B, The relative expression of senescence-, programmed cell death (PCD)-, vitamin B_6 metabolism-, starch and Suc metabolism-, and GA biosynthesis-related genes in wild-type (WT) and *bhlh2* mutant nodules at 28 dpi was quantified by RT-qPCR using *MtACTIN* as the reference gene. The error bars represent the ± SD of the means of two biological replicates, and asterisks indicate a significant difference between the wild-type and *bhlh2*-T36 nodules (Student's *t* test, $*P < 0.05$, $**P < 0.01$, $***P < 0.001$).

cis-elements, namely F1R1 (primers MtCP77-ChIP-qF1 and MtCP77-ChIP-qR1) and F3R3 (primers MtCP77-ChIP-qF3 and MtCP77-ChIP-qR3), which were upstream and downstream of F2R2, respectively, were not enriched (Fig. 6, C and D). These results indicated that the MtbHLH2 protein could bind to the *MtCP77* promoter in vivo, which suggests that MtbHLH2 could directly regulate *MtCP77* in *M. truncatula*.

MtCP77 and *MtbHLH2* Show Opposite Expression Patterns from the Meristematic Zone to the Nitrogen Fixation Zone

To explore the tissue expression pattern of *MtCP77*, the transcript levels of *MtCP77* in different tissues of *M. truncatula* R108 at 28 dpi with *S. meliloti* 1021 were analyzed by RT-qPCR. The results showed that the expression of *MtCP77* in the nodules was higher than that in the roots, stems, and leaves (Fig. 7A), which suggested that *MtCP77* might primarily function in the nodules. Putative *M. truncatula* promoter-GUS-transgenic lines were obtained by *A. tumefaciens*-mediated transformation, and a histochemical analysis of GUS staining in stable transgenic lines at 14 dpi, 28 dpi, and 42 dpi with Sm1021 was performed. The tissue expression pattern of *MtCP77* in nodules was analyzed, and the results showed that *MtCP77* was mainly expressed in the nitrogen fixation zone and vascular bundles (Fig. 7, B–D). The expression of *MtCP77* was increasingly enhanced from the meristematic zone to the nitrogen fixation zone (Fig. 7, E–G), which was consistent with the data in the Symbimics website (https://iant.toulouse.inra.fr/symbimics; Roux et al., 2014; Supplemental Fig. S3C) and opposite to the *MtbHLH2* expression pattern. These results imply that MtCP77 may be involved in nodule senescence and is inhibited by MtbHLH2.

To address the subcellular localization of MtCP77, MtCP77-eGFP alongside RFP-HDEL (endoplasmic reticulum [ER] localization marker; Zhang et al., 2015) or GONST1-RFP (Golgi localization marker; Tse et al., 2006) were transiently coexpressed in onion epidermal cells. MtCP77 colocalized with HDEL (Fig. 7H) with an ICQ of 0.402 (Supplemental Fig. S6A) and partially colocalized with GONST1 (Fig. 7I) with an ICQ of 0.316 (Supplemental Fig. S6B). Therefore, MtCP77 was found to be localized in the ER and Golgi apparatus.

MtCP77 Is a Functional Cys Protease That Plays a Positive Role in Nodule Senescence

The genomic fragment of *MtCP77* is 1672 bp in length, and this gene contains three introns (Supplemental Fig. S7A). The cDNA fragment of *MtCP77* is 1092 bp in length, and this transcript is predicted to encode a 363-amino -acid protein (Supplemental Fig. S7B). *MtCP77* belongs to the PLCP family, which is also referred to as the C1A family. The PLCP subfamilies 1 to 6 and 8 have an inconsecutive ERFNIN (ExxxRxxxFxxNxxx[I/V]xxxN) motif in the prodomain that contains an autoinhibitory domain. The PLCPs contain a catalytic triad (Cys-25-His-159-Asn-175), which implies that they are functional Cys proteases (Richau et al., 2012). Phylogenetic analysis showed that MtCP77 belongs to the CathL-like subfamily (Supplemental Fig. S7C; Supplemental Notes S2). MtCP77 contains the catalytic triad Cys-22-His-25-Asn-179, which

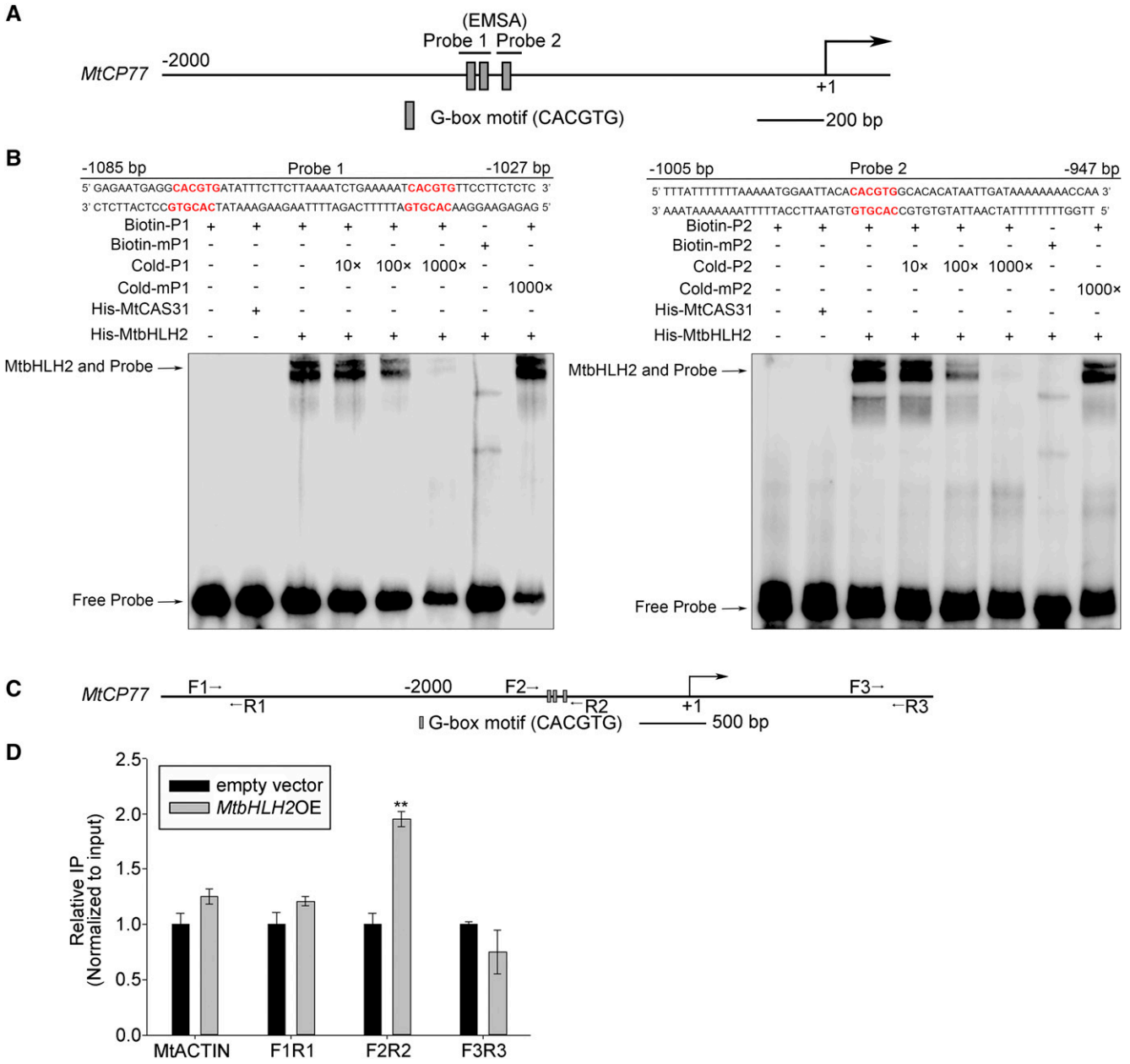

Figure 6. MtbHLH2 directly binds to the promoter of *MtCP77*. A, Schematic diagram of G-box cis-elements in the promoter of *MtCP77* for the EMSA assay. The sequence 2000 bp upstream of the transcriptional start site (ATG) and part of the coding sequence of *MtCP77* are shown. The transcriptional start site is shown at position +1. B, EMSA for the analysis of MtbHLH2 binding to G-box cis-elements in the promoter of *MtCP77*. A purified His-MtbHLH2 protein (200 ng) was incubated with biotin-labeled probes (Biotin-P1 and Biotin-P2, 20 fM) or biotin-labeled mutant probes (Biotin-mP1 and Biotin-mP2, 20 fM). For the competition assay, unlabeled probes with different concentrations (from 10 to 1000 times, Cold-P1 and Cold-P2) or unlabeled mutant probes (1000 times, Cold-mP1 and Cold-mP2) were added. mP, Mutant probe with the 5′-AAAAAA-3′ motif instead of 5′-CACGTG-3′. The G-box cis-elements are presented in bold red text. MtCAS31, a dehydrin, was used as a negative control. The numbers of bp upstream of the transcriptional start site (ATG) are indicated on the primer sequence. C, Schematic diagram of G-box cis-elements in the promoter of *MtCP77* for the ChIP assay. The approximate sequence 4000 bp upstream of the transcriptional start site (ATG) and part of the coding sequence of *MtCP77* are shown. The transcriptional start site is shown at position +1. Three pairs of primers were used for RT-qPCR: the F2/R2 pair containing the G-box cis-elements in the *MtCP77* promoter region (−1080 to −771 bp), the F1/R1 pair located upstream of the G-box cis-elements (−3622 to −3493 bp), and the F3/R3 pair located downstream of the G-box cis-elements (+1451 to +1623 bp). D, In vivo ChIP assay showing the binding of MtbHLH2 to the promoter of *MtCP77*. The ChIP assay was performed using EV-transgenic plants and *MtbHLH2*OE-transgenic plants at 28 dpi with *S. meliloti* 1021. EV-transgenic plants were used as the negative control. *MtACTIN* was used as the reference gene. The error bars represent the ± SD of the means of two independent experiments (Student's *t* test, $^{**}P < 0.01$). Three G-box cis-elements are shown by gray boxes.

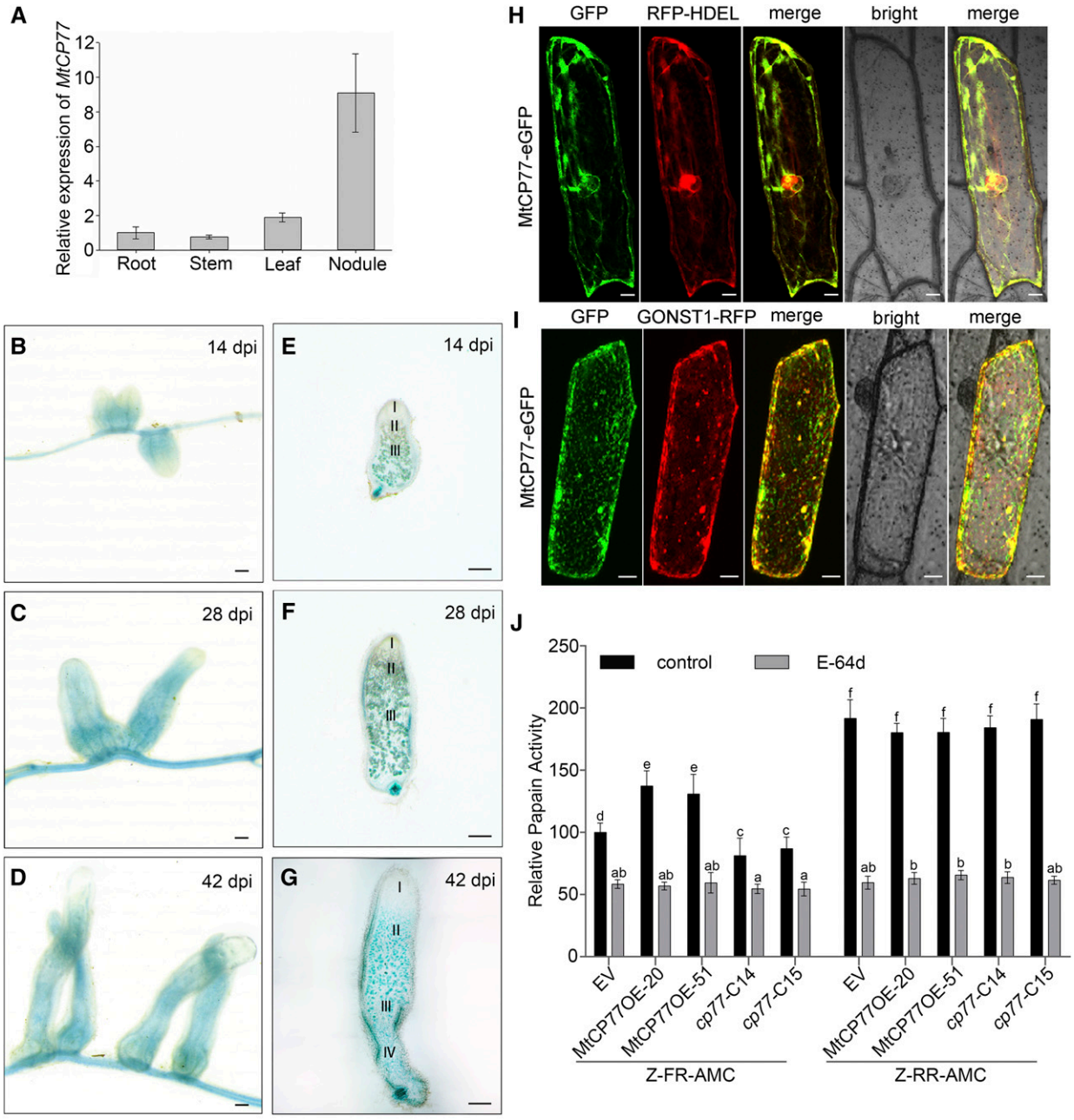

Figure 7. Expression pattern and Cys protease activity of *MtCP77*. A, The relative expression of *MtCP77* in the roots, stems, leaves, and nodules of wild-type plants at 28 dpi with *S. meliloti* 1021 was quantified by RT-qPCR using *MtACTIN* as the reference gene. The error bars represent the ± SD of the means of two biological replicates. B to G, GUS staining of *MtCP77* expressed in *M. truncatula* nodules. The expression pattern of the 2-kb promoter region of *MtCP77* was detected. B to D, GUS staining of nodules on stable transgenic plants at 14 (B), 28 (C), and 42 dpi (D). E to G, Sections of nodules at 14 (E), 28 (F), and 42 dpi (G). The section thickness is 80 μm. The different zones of the nodules (I–IV) are shown. I, Meristematic zone; II, infection zone; III, nitrogen fixation zone; IV, senescence zone. Bars = 1 mm. H and I, Subcellular localization of MtCP77 in onion epidermal cells. MtCP77-eGFP fusion protein driven by the CaMV35S promoter was transiently coexpressed with RFP-HDEL (ER marker, H) and GONST1-RFP (Golgi marker, I) in onion epidermal cells via particle bombardment. The fluorescence signals, i.e. GFP and RFP, were detected by CLSM using excitation wavelengths of 488 nm and 546 nm, respectively. Bars = 20 μm. J, The Cys protease activity of MtCP77 in EV, *MtCP77*OE, and *Mtcp77*. The protein extracts of roots of EV, *MtCP77*OE, and *Mtcp77* at 14 dpi were used to characterize their proteinase activity. The Cys activity of MtCP77 was assayed for Z-FR-AMC (cathepsin-L) and Z-RR-AMC (cathepsin-B) proteolytic activity, and the papain inhibitor E-64d was used to inhibit the Cys protease activity. The data are represented as a percentage of the Z-FR-AMC proteolytic activity of the *EV*. The error bars represent the means ± SD of three biological replicates, and significant differences were determined with ANOVA with a post-hoc Tukey test and are indicated by letters ($P < 0.05$).

is not a typical catalytic triad and shows a change in the His position; however, this Cys-22-His-25-Asn-179 triad was mutually adjacent according to the predicted protein structure (Supplemental Fig. S7D), suggesting that MtCP77 is likely a functional Cys protease.

To elucidate the biological functions of MtCP77 in nodule senescence, transgenic *M. truncatula* lines overexpressing *MtCP77* and *Empty Vector* (*EV*) were obtained by *A. tumefaciens*-mediated transformation. Three stable transgenic lines (*MtCP77*OE-20, *MtCP77*OE-44, and *MtCP77*OE-51) were selected following RT-qPCR and western blotting analysis (Supplemental Fig. S8). Furthermore, *MtCP77*-knockout mutants were generated using clustered regularly interspaced short palindromic repeats/CRISPR-associated protein 9 (CRISPR/Cas9) technology via *A. tumefaciens*-mediated transformation. The transgenic plants were identified by sequencing. The *cp77*-C14-knockout mutant containing a 4-bp deletion triggered the frameshift mutation (Supplemental Fig. S9). The *cp77*-C15- and *cp77*-C30-knockout mutants contained a guanine (G) insertion and an adenine (A) insertion, respectively, which led to an insertion mutation (Supplemental Fig. S9). Overall, these overexpression lines and mutants were suitable to analyze the biological function of MtCP77.

The Cys protease activity of MtCP77 in EV, *MtCP77*OE, and *Mtcp77* was assayed with Z-FR-AMC (cathepsin-L activity) and Z-RR-AMC (cathepsin-B activity), two papain substrates. Compared that in the *EV* root lines, Z-FR-AMC proteolytic activity was significantly increased with the overexpression of *MtCP77* and decreased with the mutation of *MtCP77*, whereas no significant difference in Z-RR-AMC proteolytic activity was observed (Fig. 7J). Furthermore, both Z-FR-AMC and Z-RR-AMC proteolytic activity were inhibited in the presence of the papain inhibitor E-64d (Fig. 7J). These results indicated that MtCP77 is a functional CathL-like Cys protease and imply that MtCP6 is involved in the nodule senescence process.

The nodule developmental phenotype and nitrogenase activity assays showed that the overexpression of *MtCP77* led to an acceleration of nodule senescence and a decline in nitrogenase activity (Fig. 8, A, B, and E), which is consistent with the findings obtained for *bhlh2* mutants. At 49 dpi, the wild-type nodules were green, which suggested that the nodules had entered the senescence stage, and the *cp77* nodules were pink (Fig. 8D). The nitrogenase activity of *cp77* nodules was significantly higher than that of the wild-type nodules, as demonstrated by the ARA (Fig. 8F). In summary, the mutation of *MtCP77* delays nodule senescence.

MtbHLH2 and MtCP77 Play Opposite Roles in Plant PCD and ROS Accumulation during Nodule Senescence

To determine whether MtbHLH2 and MtCP77 can affect plant PCD and reactive oxygen species (ROS) accumulation, a terminal deoxynucleotidyl transferase (TdT)-mediated dUTP nick end labeling (TUNEL) assay and 3,3′-diaminobenzidine (DAB) staining were performed. Wild type, *bhlh2* mutant, EV, and *MtCP77*OE nodules were used for DAB staining at 28 dpi. Compared with the wild-type or EV nodules, the *bhlh2* and *MtCP77*OE nodules presented higher concentrations of hydrogen peroxide (H_2O_2; Fig. 9, A and B). Additionally, a TUNEL assay, which was used to detect PCD events in plant tissues with cell death signals, showed that the *bhlh2* nodules exhibited strong DNA fragmentation at 28 dpi compared with the wild-type nodules (Fig. 9, C and E), and weaker staining of DNA fragmentation was observed in the *cp77* nodules than in the wild-type nodules at 49 dpi (Fig. 9, D and F). Therefore, MtbHLH2 and MtCP77 play opposite roles in plant PCD and ROS accumulation during nodule senescence.

MtbHLH2 Represses the Expression of *MtCP77* to Prevent Early Nodule Senescence in *M. truncatula*

To confirm that endogenous MtbHLH2 can repress the expression of *MtCP77*, *ProMtCP77*:*GUS* was inserted by *Agrobacterium rhizogenes*-mediated hairy root transformation (Supplemental Fig. S10). The construct was expressed in the wild-type and *bhlh2* nodules, and an immunoblot analysis was performed to test the protein level of GUS using GFP-FLAG as the loading control. GUS was barely detectable in *ProMtCP77*:*GUS*/wild type and strongly expressed in *ProMtCP77*:*GUS*/*bhlh2*-T36, *ProMtCP77*:*GUS*/*bhlh2*-T43, and *ProMtCP77*:*GUS*/NF13601 (Fig. 10A). In addition, GUS staining of *ProMtCP77*:*GUS/bhlh2-T36* showed that, apart from nitrogen fixation and senescence zone, GUS was expressed in the meristematic zone (Fig. 10, B and C), similar to *ProMtCP77*:*GUS*/wild type. Thus, endogenous MtbHLH2 suppresses the expression of *MtCP77* with respect to both expression level and expression tissue area in nodules. We further compared the expression pattern of *MtCP77* in wild type and *bhlh2*-TALEN mutants at different stages of nodule development. RT-qPCR analysis confirmed that during nodule development, the relative expression of *MtCP77* progressively increased until it reached a peak at 28 dpi and then gradually decreased. The expression of *MtCP77* in the *bhlh2* nodules was always higher than that in the wild-type nodules and significantly higher than that in the wild-type nodules at 28 dpi (Fig. 10D). These results imply that MtbHLH2 can repress the expression of *MtCP77* at different stages of nodule development.

In this study, we found a repressive transcription factor, MtbHLH2, that negatively regulates nodule senescence, and mutants defective in MtbHLH2 show premature senescence and decreased nitrogenase activity. In the nodules, the expression of *MtbHLH2* and *MtCP77* gradually decreased and increased, respectively, from the meristematic zone to the nitrogen fixation zone. The binding of MtbHLH2 to the

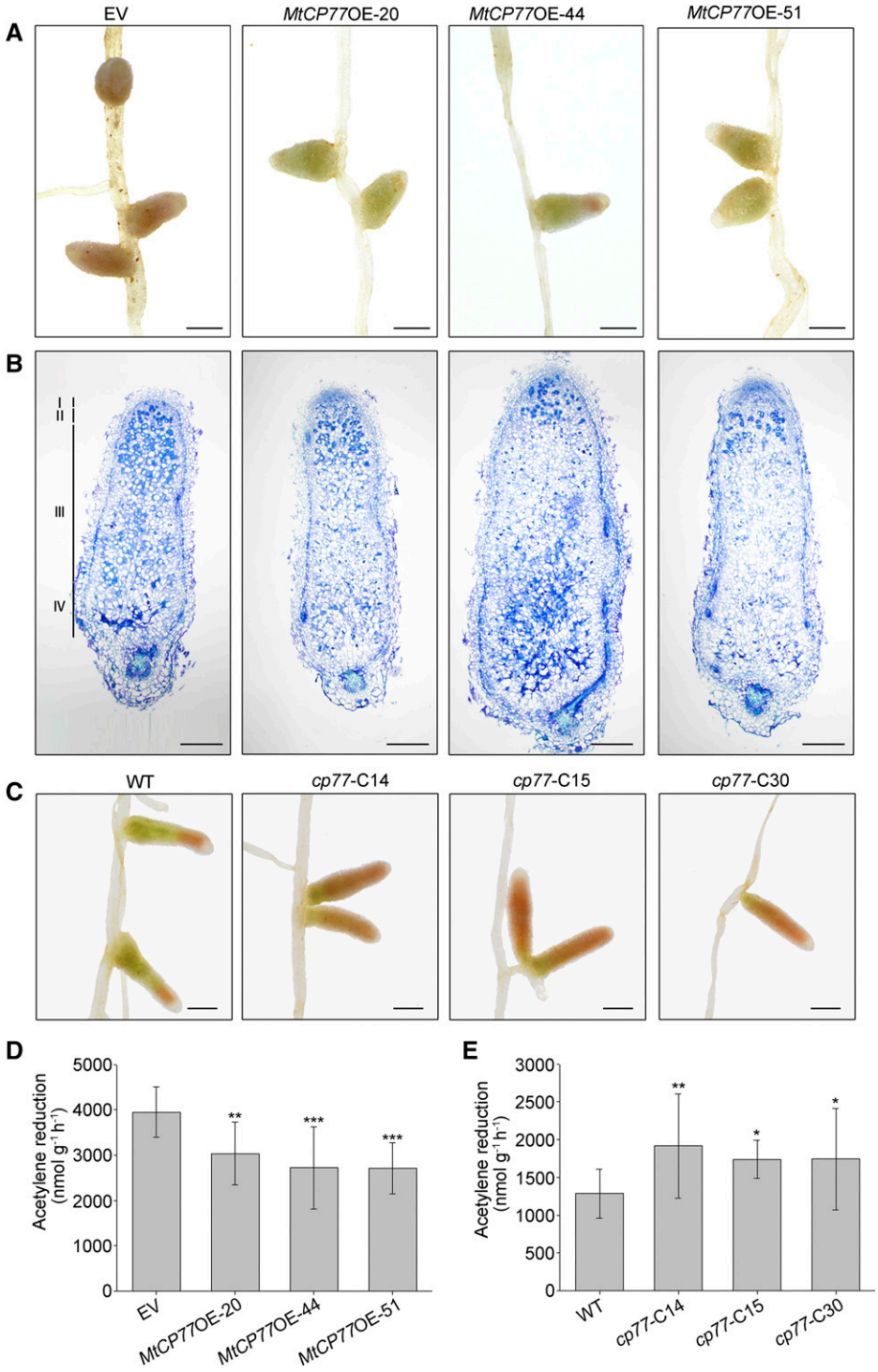

Figure 8. MtCP77 positively regulates nodule senescence. A, Light micrographs of nodules in EV-transgenic plants and *MtCP77*OE-transgenic plants at 28 dpi. Bars = 1 mm. B, Longitudinal sections of toluidine blue-stained nodules in EV-transgenic plants and *MtCP77*OE-transgenic plants at 28 dpi. The section thickness is 8 μm. The different zones of the nodules (I–IV) are shown. I, Meristematic zone; II, infection zone; III, nitrogen fixation zone; IV, senescence zone. Bars = 200 μm. C, Light micrographs of wild-type (WT) and *cp77* mutant nodules at 49 dpi. Bars = 1 mm. D, The nitrogenase activity of EV-transgenic and *MtCP77*OE-transgenic plant nodules at 28 dpi was determined by an ARA. The error bars represent the ± SD of the means, and asterisks indicate a significant difference between the EV and *MtCP77*OE-transgenic plants (one-way ANOVA followed by Tukey's post-hoc test, $^{**}P < 0.01$, $^{***}P < 0.001$, $n = 19$). E, The nitrogenase activity of the wild-type and *cp77* nodules at 49 dpi was determined by an ARA. The error bars represent the ± SD of the means, and asterisks indicate a significant difference between the wild-type and *cp77* mutant nodules (one-way ANOVA followed by Tukey's post-hoc test, $^{*}P < 0.05$, $^{**}P < 0.01$, $n \geq 15$).

promoter of *MtCP77* inhibited *MtCP77* expression to delay nodule senescence, which suggests that MtbHLH2 can prevent early nodule senescence to ensure effective nitrogen fixation by inhibiting the expression of *MtCP77* (Fig. 10E). Taken together, the results show that MtbHLH2 is a negative regulator of nodule senescence and inhibits the expression of *MtCP77*, which positively modulates plant PCD, ROS accumulation, and nodule senescence in *M. truncatula*.

DISCUSSION

Approximately 100 bHLH genes exist in the *M. truncatula* genome (Young et al., 2011), and to date, only two legume bHLHs related to nodulation have been

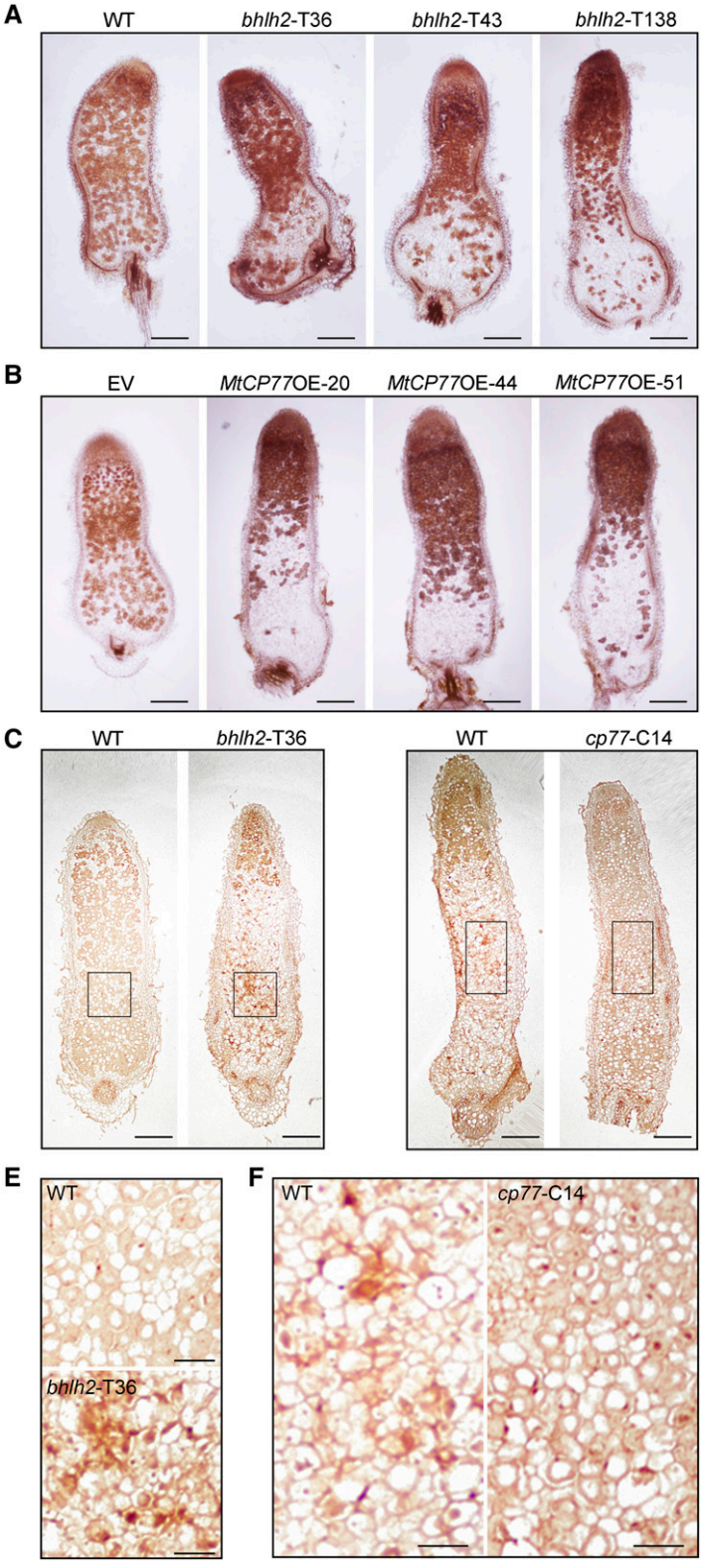

Figure 9. MtbHLH2 and MtCP77 play opposing roles in plant PCD and ROS accumulation. A and B, The accumulation of H_2O_2 in longitudinal sections of *bhlh2* (A) or *MtCP77*OE nodules (B) at 28 dpi was detected. A higher concentration of H_2O_2 was found in the *bhlh2* (A) or *MtCP77*OE nodules (B). Bars = 200 μm. C and D, DNA fragmentation in longitudinal sections of wild-type (WT) and *bhlh2* nodules at 28 dpi (C) or wild-type and *cp77* nodules at 49 dpi (D) was detected by TUNEL assay. DNA

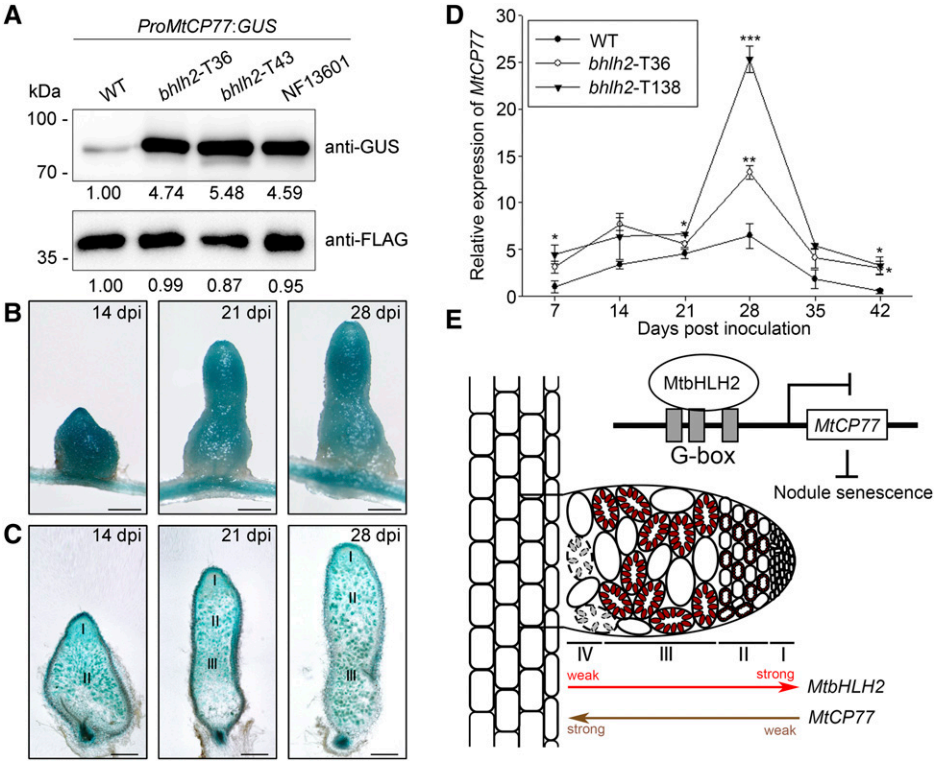

Figure 10. MtbHLH2 represses the expression of *MtCP77*. A, MtbHLH2 represses the expression of *MtCP77* in *M. truncatula*. The 2-kb promoter region of *MtCP77* was used for this assay. *ProMtCP77*:*GUS*, which carried an expression box of GFP-FLAG under the control of the CaMV35S promoter, was transformed into the wild type (WT) and *bhlh2* mutants (*bhlh2*-T36, *bhlh2*-T43, and NF13601) by *A. rhizogenes*-mediated hairy root transformation. Composite transgenic plants were harvested, and proteins were extracted from *ProMtCP77*:*GUS*/wild type, *ProMtCP77*:*GUS*/*bhlh2*-T36, *ProMtCP77*:*GUS*/*bhlh2*-T43, and *ProMtCP77*:*GUS*/NF13601 for immunoblot analysis. GFP-FLAG was used as a loading control. ImageJ software was used to quantify the immunoblot bands. B and C, GUS staining of *MtCP77* expression in the nodules of *ProMtCP77*:*GUS*/*bhlh2*-T36. B, GUS staining of nodules on *ProMtCP77*:*GUS*/*bhlh2*-T36 hairy roots at 14, 21, and 28 dpi. C, Sections of nodules at 14, 21, and 28 dpi. The section thickness is 80 μm. The different zones of the nodules (I–III) are shown. Bars = 1 mm. D, The relative expression of *MtCP77* in wild-type and *bhlh2* mutant nodules (*bhlh2*-T36 and *bhlh2*-T138) at different time points after inoculation (7, 14, 21, 28, 35, and 42 dpi) with *S. meliloti* 1021 was quantified by RT-qPCR using *MtACTIN* as the reference gene. The error bars represent the ± SD of the means of two biological replicates, and asterisks indicate a significant difference between the wild-type and *bhlh2* mutant nodules (one-way ANOVA followed by Tukey's post-hoc test, $*P < 0.05$, $**P < 0.01$, $***P < 0.001$). E, A proposed model for the regulation of MtbHLH2 during nodule senescence in *M. truncatula*. In the nodules, the expression of *MtbHLH2* gradually decreases from the meristematic zone to the nitrogen fixation zone, whereas the expression of *MtCP77* gradually increases. The binding of MtbHLH2 to the promoter of *MtCP77* inhibits *MtCP77* expression to delay nodule senescence. The different zones of the nodules (I–IV) are shown. I, Meristematic zone; II, infection zone; III, nitrogen fixation zone; IV, senescence zone.

reported. GmSAT1, which is also called GmbHLHm1, encodes a symbiotic ammonium transporter and is associated with nodule development and NH_4^+ transport (Kaiser et al., 1998; Marini et al., 2000; Chiasson et al., 2014). MtbHLH1, which is particularly expressed in the roots and nodules, exerts a critical influence on nodule vascular patterning and nodule-to-plant nutrient exchange (Godiard et al., 2011). However, bHLH transcription factors involved in nodule senescence have not yet been identified in *M. truncatula*. In this study, mutants showing early nodule senescence were identified, and the gene responsible for this process was *MtbHLH2* (Figs. 1 and 2).

The analysis of transcriptome data indicated that MtbHLH2 regulates vitamin B_6 metabolism (Supplemental Fig. S4A). As an important cofactor, vitamin B_6 is involved in many biochemical reactions, including decarboxylation, transamination, elimination, racemization,

Figure 9. (*Continued.*)
fragmentation resulting from the cell death signaling cascade is shown as brown signals in both plant nuclei and rhizobia of *bhlh2* nodules at 28 dpi (C) or wild-type nodules at 49 dpi (D). Bars = 200 μm. E and F, Magnification of the boxed areas in (C) and (D). Bars = 50 μm.

and transsulfuration reactions, which are mainly related to the synthesis of amino acids (Drewke and Leistner, 2001). The active forms of vitamin B_6 are pyridoxal-5-phosphate and pyridoxamine-5-phosphate, which act as cofactors of many enzymes involved in the metabolism of amino acids. In this study, *MtDMPP950* and *MtDMPP910*, which encode 2,3-diketo-5-methylthio-1-phosphopentane phosphatases, were upregulated in the *bhlh2* mutant nodules at 28 dpi compared with that in the wild-type nodules (Fig. 5B). These enzymes convert pyridoxal-5-phosphate and pyridoxamine-5-phosphate into pyridoxal and pyridoxamine, respectively, and thereby hinder amino acid synthesis. These results suggest that MtbHLH2 might also be involved in nodule senescence by affecting the synthesis of amino acids.

The analysis of transcriptome data also showed that MtbHLH2 modulates diterpenoid biosynthesis, which was found to be associated with GA biosynthesis (Supplemental Fig. S4A). Ent-kaurene synthase, cytochrome P450 family ent-kaurenoic acid oxidase (KAO), and GA 2-beta-dioxygenase (also called GA 2-oxidase, MtGA2ox) are the key enzymes in the GA biosynthetic pathway (Sun, 2008), and the transcriptome data obtained in this study showed that these enzymes were upregulated in the *bhlh2* mutant nodules. The RT-qPCR results also showed that *MtKAO230* and *MtKAO240* were significantly upregulated in the *bhlh2* mutant nodules (Fig. 5B), and these enzymes are associated with the first steps of GA biosynthesis and promote the generation of GA_{12}, the common precursor of all types of GAs in plants (Hedden and Phillips, 2000). Previous studies have reported that GA might inhibit nodule senescence (Van de Velde et al., 2006; Serova et al., 2019), so the up-regulation of *MtKAO230* and *MtKAO240* appeared to contradict the phenotype of *bhlh2*. However, the transcriptome data obtained in this study also indicated that *MtGA2ox* was upregulated in *bhlh2* (Supplemental Fig. S11), and this up-regulation might result in conversion of the bioactive form of GA into the inactive form to maintain GA homeostasis in *bhlh2*. These results suggest that the regulation of GA biosynthesis might also be involved in the nodule senescence processes regulated by bHLH2.

The target gene *MtCP77*, which is modulated by MtbHLH2, was identified by transcriptome sequencing. The expression of *MtCP77* in nodules was higher than that in roots, stems, and leaves (Fig. 7A), which suggested that MtCP77 might play a crucial role in root nodules. This study showed that the overexpression of *MtCP77* decreased the nitrogen fixation abilities of nodules and promoted nodule senescence (Fig. 8, A, B, and D), and the *cp77* mutants exhibited the opposite phenotype (Fig. 8, C and E). In agreement with previous studies, the knockdown of *AsNodf32*, a *PLCP*, delayed nodule senescence (Li et al., 2008), and the down-regulation of *MtCP6* increased the nitrogen fixation abilities of nodules and delayed nodule senescence; moreover, the overexpression of *MtCP6* accelerated nodule senescence (Pierre et al., 2014). Additionally, the overexpression of *MtCP77* triggered a decrease in nitrogenase activity and high concentrations of hydrogen peroxide (H_2O_2; Figs. 8D and 9B), and the mutation of *MtCP77* resulted in an increase in nitrogenase activity and a reduction in DNA fragmentation (Figs. 8E and 9, D and F), which suggested the occurrence of PCD and ROS accumulation during nodule senescence. These results were similar to those obtained in previous studies, which showed that PCD events could be regarded as the initiation of senescence (Alesandrini et al., 2003). The ROS that were accumulated in response to *MtCP77* overexpression (Fig. 9B) might produce highly oxidizing conditions to result in nodule senescence, which implies the occurrence of a redox shift in the nodules from a highly reducing status, which is required for nitrogen fixation in nodules, to highly oxidizing conditions, which might lead to senescence (Puppo et al., 2005).

Many endogenous plant Cys proteases are located in the vacuole (Callis, 1995). Many vacuolar proteases are transported from the ER to the vacuole through the Golgi apparatus, and this transport is a Golgi-dependent pathway (Okamoto, 2006; Xiang et al., 2013). In general, PLCPs that do not contain ER retention signal Lys-Asp-Glu-Leu-tail Cys proteases are first transported from the ER to the Golgi apparatus and are then recognized by vacuolar sorting receptor on the Golgi apparatus, leading to the transport of proenzymes to the vacuoles. During or after transport to the vacuoles, the proenzymes are converted into mature enzymes via proteolytic processing (Okamoto, 2006). This study revealed that MtCP77 is localized in the ER and Golgi apparatus (Fig. 7, H and I), which might be due to the presence of the full-length coding sequence of *MtCP77* as a proenzyme in the onions and its inability to be transported to the vacuoles without undergoing proteolysis and becoming a mature enzyme. The subcellular localization of MtCP77 in *M. truncatula* should be further studied.

In conclusion, this study describes an important regulatory module of nodule senescence, namely MtbHLH2-MtCP77, that is associated with plant PCD and ROS accumulation and ultimately leads to nodule senescence.

MATERIALS AND METHODS

Plant Materials and Growth Conditions

The *Medicago truncatula* ecotype R108 was used as the wild-type material in all the experiments performed in this study. Both *bhlh2 Tnt1*-insertion mutants were isolated from the *M. truncatula* mutant database (primers are listed in Supplemental Table S2). The T1 generation *bhlh2 Tnt1*-insertion mutants were used for phenotypic experiments.

The full-length coding sequences of *MtbHLH2* and *MtCP77* were cloned into pCAMBIA1307-FLAG (primers are listed in Supplemental Table S2). Stable transgenic plants were obtained by *Agrobacterium tumefaciens*-mediated transformation as previously described (Cosson et al., 2006).

Seeds were sterilized for germination as described previously (Duan et al., 2017). For nodule sectioning and the ARA, seedlings were grown on Fåhraeus solid and liquid media (Fåhraeus, 1957) without nitrogen (pH 6.5) in square dishes and containing a vermiculite:perlite (5:2, v/v) mixture, respectively. For

all the experiments, the plants were incubated in a growth chamber at 24°C with a 16-h light/8-h dark cycle and 70% relative humidity.

RNA Extraction and RT-qPCR

Total RNA was extracted using the TRIzol reagent (Invitrogen), and 2 μg of total RNA was used for reverse transcription. The RT-qPCR analysis was performed using a CFX-96 Real-Time System (Bio-Rad) with TB Green Premix ExTaq (TaKaRa). To verify the expected stable expression of the reference genes during nodule development, the stability of four candidate reference genes (*MtACTIN*, *MtACTIN11*, *MtH3L*, and *MtRBP1*) at different time points after inoculation with *Sinorhizobium meliloti* 1021 was assessed using geNorm software (Vandesompele et al., 2002). The expression of *MtACTIN* was stable at the lowest *M* value ($M = 0.047 < 0.5$). *MtACTIN* was selected as the reference gene, and the relative expression data were normalized to *MtACTIN* expression. The mean and SD values were calculated from the results of two biological replicates. The primers used in this study are listed in Supplemental Table S2. *MtACTIN11*, *MtH3L*, and *MtRBP1* genes were used as references (Plet et al., 2011).

Rhizobial Inoculation and ARA

Seven-day-old seedlings were inoculated with *S. meliloti* 1021 for the nodulation assay, and the nitrogen fixation ability of rhizobia was measured using an ARA as previously described (Li et al., 2018).

Histochemical GUS Staining

The 2.3-kb promoter of *MtbHLH2* and the 2-kb promoter of *MtCP77* upstream of the transcriptional start site (ATG) were amplified by PCR from *M. truncatula* genomic DNA and cloned into pCAMBIA1381 carrying the *GUS* reporter gene (primers are listed in Supplemental Table S2). The transgenic plants were stained as previously described (Li et al., 2018).

Microscopic Analysis

Nodules were fixed overnight at 4°C with formalin-acetic-alcohol (50% [v/v] ethanol, 5% [v/v] acetic acid, and 3.7% [v/v] formalin) solution. The fixed materials were dehydrated in an ethanol series and subsequently embedded in Paraplast (Sigma). Longitudinal sections (8 μm) were prepared using an RM2235 microtome (Leica) and stained with 0.5% (w/v) toluidine blue for 10 min. The nodules for GUS staining were embedded in 6% (w/v) agarose, and longitudinal sections (80 μm) were cut using a VT1000S vibratome (Leica). The sections were photographed using a light microscope (Olympus BX51).

For electron microscopy analysis, the nodules were fixed in 2.5% (v/v) glutaraldehyde, washed three times with phosphate buffer (pH 7.2), fixed in 1% (v/v) osmic acid, washed three more times, dehydrated in an acetone series, and embedded with a Spurr Embedding Kit. Serial sections were prepared using a UC6 microtome (Leica) equipped with a diamond knife, and the sections were photographed using a JEOL JEM-1230 transmission electron microscope.

Subcellular Localization and Confocal Microscopy

MtbHLH2-GFP, MtCP77-GFP with RFP-HDEL (ER), and GONST1-RFP (Golgi marker) were transiently expressed or coexpressed in onion (*Allium cepa*) epidermal cells as previously described (Duan et al., 2017). The intensity correlation analysis was described previously (Li et al., 2004). The ICQ is based on nonparametric test analysis of the product of the differences from the mean (PDM) values: $-0.5 \leq \text{ICQ} < 0$, segregated staining; ICQ ~ 0, random staining; $0 < \text{ICQ} \leq +0.5$, dependent staining. The samples were photographed using a confocal laser scanning microscope (CLSM, Olympus FluoView FV1000).

Nuclear/Cytoplasmic Fraction and Immunoblot Assays

A. tumefaciens EHA105 carrying the MYC-MtbHLH2 plasmid was infiltrated into *Nicotiana benthamiana* leaves (primers are listed in Supplemental Table S2). Three-day-infiltration samples were extracted as previously described (Du et al., 2015). An immunoblot analysis was performed with anti-MYC (Sigma), antihistone H3 (Agrisera, nuclear fraction marker), and anticFBPase (Agrisera, cytosolic fraction marker).

Analysis of Transcriptional Activation or Repression in Yeast Cells and *N. benthamiana* Leaves

MtbHLH2 was cloned into the pGBKT7 vector, and yeast transcriptional activation was performed as previously described (Shan et al., 2012). DBD-MtbHLH2 was cloned into pCAMBIA1302, and an assay of transcriptional repression in *N. benthamiana* leaves was performed as previously described (Tao et al., 2013; primers are listed in Supplemental Table S2).

Design, Assembly, and Identification of TALEN Constructs of *MtbHLH2*

The target sequence of *MtbHLH2* was designed using TAL Effector Nucleotide Targeter 2.0 (https://tale-nt.cac.cornell.edu/) as previously described (Ma et al., 2015). The two target sequences of *MtbHLH2* had 16 and 19 repeat-variable diresidues, which were assembled by the three-step golden gate method as previously described (Cermak et al., 2011) and added to the pCAMBIA1300 vector (primers listed in Supplemental Table S2). The T1 generation *bhlh2*-TALEN mutants are used for phenotypic experiments.

Transcriptome Analysis

Sequencing was carried out by Novogene. At 28 dpi, wild-type and *bhlh2*-T36 nodules were used for digital high-throughput RNA-seq gene expression profiling, and 3 μg of total RNA per sample was then used to generate non-directional Illumina sequencing libraries. Each library was generated using the SE50 single-read sequencing method with the Illumina HiSeq 2500 platform. The gene annotation files were referenced against the *M. truncatula* genome (version 4.0) and downloaded from the J. Craig Venter Institute (http://www.jcvi.org/medicago/). Genes with an adjusted *P* value ≤ 0.05 were considered differentially expressed. The significantly enriched GO terms were analyzed using the GOseq R package (Young et al., 2010). The statistical analysis of KEGG pathway enrichment was performed using KOBAS software (Mao et al., 2005).

Protein Purification and EMSA

His-MtbHLH2 was expressed in *Escherichia coli* BL21 and purified by Ni affinity chromatography according to the manufacturer's instructions. Electrophoretic mobility shift assay (EMSA) experiments were performed using a LightShift Chemiluminescent EMSA kit (Thermo Fisher) as previously described (Duan et al., 2017; primers are listed in Supplemental Table S2).

Hairy Root Transformation and Immunoblot Assays

ProMtCP77:*GUS* carried an expression box, GFP-FLAG, driven by the CaMV35S promoter, which was used as a loading control (primers listed in Supplemental Table S2). Composite transgenic plants of wild type and *bhlh2* mutants were created by *Agrobacterium rhizogenes*-mediated hairy root transformation as previously described (Boisson-Dernier et al., 2001). Immunoblot analysis was performed with anti-GUS (Sigma) and anti-FLAG (Sigma).

Design and Identification of CRISPR/Cas9 Constructs of MtCP77

The target site of *MtCP77* was designed using CRISPR-PLANT (https://www.genome.arizona.edu/crispr/CRISPRsearch.html). The length of each of the two target sites of *MtCP77* was 19 bp. The PCR fragment was amplified from pCBC-DT1T2, and the purified PCR fragment (T1T2-PCR), combined with the binary vector pHSE401, was established by restriction-ligation reactions as previously described (Xing et al., 2014; primers are listed in Supplemental Table S2). The T1 generation of *cp77*-Cas9 mutants are used for phenotypic experiments.

Cys Protease Enzymatic Activities

The Cys protease enzymatic activities were determined as in a previous report (Pierre et al., 2014). The 14-dpi roots were harvested, and the total protein was extracted. The extraction buffer contained 50 mM Tris, pH 8, 5 mM EDTA, 20 mM NaCl, and 10% (v/v) glycerol. A Bradford protein assay (Bio-Rad) was

used to quantify the protein concentrations. N-acetyl-FR7-amido-4-methylcoumarin (Sigma, #C9521) and N-acetyl-RR7-amido-4-methylcoumarin (Sigma, #C5429) were used as substrates to assay cathepsin-L and cathepsin-B activity, respectively. The reaction mix contained 100 mM sodium acetate (pH 5.5), 1 mM EDTA, 1 mM dithiothreitol, 10 μg/mL total protein and 50 μM of substrate and was incubated at 28°C for 20 min; the papain inhibitor E-64d (Sigma, #E8640) was used as a negative control. Then, the proteolytic product, coumarin, was assayed with a spectrofluorimeter (Hitachi F-7000) at a 380-nm excitation wavelength and a 460-nm emission wavelength. Activity was measured as cleavage of substrate over time, and its values were expressed as Δ(fluorescence).min^{-1}.

ChIP

ChIP was performed as described previously (Saleh et al., 2008), with some modifications (Zhang et al., 2016; Duan et al., 2017). At 28 dpi, 2.5 g root and nodule samples were cross linked and then sonicated using a Bioruptor Plus (Diagenode; low power, on for 60 s, off for 60 s, four cycles). Anti-FLAG (Sigma) was used to immunoprecipitate the target MtbHLH2-FLAG fusion protein. The enriched DNA fragments that contrasted with the input samples were detected by RT-qPCR (primers are listed in Supplemental Table S2) using *MtACTIN* as the negative control.

DAB Staining and TUNEL Assay

At 28 dpi, nodules were collected for DAB staining as previously described (Zhou et al., 2015). At 28 or 49 dpi, nodules were fixed in formalin-acetic-alcohol solution, and TUNEL assays were performed using the DeadEnd Colorimetric TUNEL System (Promega) according to the manufacturer's instructions.

Phylogenetic Analysis

Protein sequences of bHLH transcription factors or PLCPs in *M. truncatula* and Arabidopsis (*Arabidopsis thaliana*) were obtained from the JCVI and TAIR databases, respectively. The multiple sequence alignment was analyzed using ClustalW2 software (Larkin et al., 2007) or the MAFFT online service (Katoh et al., 2002, 2017), and a phylogenetic tree was generated using PhyML with the neighbor-joining method or the maximum likelihood method (Guindon et al., 2010). The numbers on the branches show bootstrap values based on 1000 replicates. The phylogenetic analysis was performed using EvolView (Zhang et al., 2012a).

Statistical Analysis

All data analyses and calculations of the means and SD were performed using Sigma Plot 12.0 and Microsoft Excel 2010. The statistical significance of the differences was assessed by Student's *t* test or one-way ANOVA followed by Tukey's post-hoc test using SPSS software (version 16.0). The *P* values for each statistical test are reported.

Accession Numbers

The sequence data obtained in this study can be found in the GenBank data library under the accession numbers MK798038 (MtbHLH2) and MK798039 (MtCP77). The raw data used for the RNA-seq analysis have been submitted to the NCBI database under the accession number PRJNA383274.

Supplemental Data

The following supplemental materials are available.

Supplemental Figure S1. Schematic diagram of the domain structure in MtbHLH2 and phylogenetic analysis of *MtbHLH2*.

Supplemental Figure S2. Analysis of the intensity of the colocalization of MtbHLH2 with the nuclear dye DAPI.

Supplemental Figure S3. Expression patterns of *MtbHLH2* and *MtCP77*.

Supplemental Figure S4. Analysis of pathways enriched with differentially expressed genes regulated by MtbHLH2.

Supplemental Figure S5. Molecular identification of *MtbHLH2*OE-transgenic plants.

Supplemental Figure S6. Analysis of the intensity of the colocalization of MtCP77 with an ER marker and a Golgi marker.

Supplemental Figure S7. Gene structure and phylogenetic analysis of *MtCP77*.

Supplemental Figure S8. Molecular identification of *MtCP77*OE-transgenic plants.

Supplemental Figure S9. The sequence of *MtCP77* in *cp77*-C after editing by CRISPR/Cas9.

Supplemental Figure S10. Schematic diagram of the *ProMtCP77:GUS* construct.

Supplemental Figure S11. The expression of *GA2ox1* and *GA2ox2* in nodules of R108 and *bhlh2-1*.

Supplemental Table S1. Analysis of upregulated gene expression profiles from RNA-seq data used for RT-qPCR.

Supplemental Table S2. List of primers used in this study.

Supplemental Notes S1. The protein sequences of bHLH transcription factors in *M. truncatula* and Arabidopsis that were used as an input for the phylogenetic tree analysis.

Supplemental Notes S2. The protein sequences of PLCPs in *M. truncatula* and Arabidopsis that were used as an input for the phylogenetic tree analysis.

ACKNOWLEDGMENTS

The authors thank Dr. Genji Qin (State Key Laboratory of Protein and Plant Gene Research, College of Life Sciences, Peking University, China) for kindly providing 35S-UAS-GUS vector used in this study. The authors also thank Dr. Qijun Chen (State Key Laboratory of Plant Physiology and Biochemistry, College of Biological Sciences, China Agricultural University, China) for kindly providing CRISPR/Cas9 vector used in this study.

Received May 13, 2019; accepted September 23, 2019; published October 7, 2019.

LITERATURE CITED

Alesandrini F, Mathis R, Van de Sype G, Herouart D, Puppo A (2003) Possible roles for a cysteine protease and hydrogen peroxide in soybean nodule development and senescence. New Phytol **158:** 131–138

Berger A, Boscari A, Frendo P, Brouquisse R (2019) Nitric oxide signaling, metabolism and toxicity in nitrogen-fixing symbiosis. J Exp Bot **70:** 4505–4520

Berrabah F, Balliau T, Aït-Salem EH, George J, Zivy M, Ratet P, Gourion B (2018) Control of the ethylene signaling pathway prevents plant defenses during intracellular accommodation of the rhizobia. New Phytol **219:** 310–323

Berrabah F, Bourcy M, Eschstruth A, Cayrel A, Guefrachi I, Mergaert P, Wen J, Jean V, Mysore KS, Gourion B, et al (2014) A nonRD receptor-like kinase prevents nodule early senescence and defense-like reactions during symbiosis. New Phytol **203:** 1305–1314

Boisson-Dernier A, Chabaud M, Garcia F, Bécard G, Rosenberg C, Barker DG (2001) *Agrobacterium rhizogenes*-transformed roots of *Medicago truncatula* for the study of nitrogen-fixing and endomycorrhizal symbiotic associations. Mol Plant Microbe Interact **14:** 695–700

Bourcy M, Brocard L, Pislariu CI, Cosson V, Mergaert P, Tadege M, Mysore KS, Udvardi MK, Gourion B, Ratet P (2013) *Medicago truncatula* DNF2 is a PI-PLC-XD-containing protein required for bacteroid persistence and prevention of nodule early senescence and defense-like reactions. New Phytol **197:** 1250–1261

Buchanan-Wollaston V, Page T, Harrison E, Breeze E, Lim PO, Nam HG, Lin JF, Wu SH, Swidzinski J, Ishizaki K, et al (2005) Comparative transcriptome analysis reveals significant differences in gene expression and signalling pathways between developmental and dark/starvation-induced senescence in *Arabidopsis*. Plant J **42:** 567–585

Callis J (1995) Regulation of protein degradation. Plant Cell **7:** 845–857

Cam Y, Pierre O, Boncompagni E, Hérouart D, Meilhoc E, Bruand C (2012) Nitric oxide (NO): A key player in the senescence of *Medicago truncatula* root nodules. New Phytol **196:** 548–560

Cermak T, Doyle EL, Christian M, Wang L, Zhang Y, Schmidt C, Baller JA, Somia NV, Bogdanove AJ, Voytas DF (2011) Efficient design and assembly of custom TALEN and other TAL effector-based constructs for DNA targeting. Nucleic Acids Res **39:** e82

Chiasson DM, Loughlin PC, Mazurkiewicz D, Mohammadidehcheshmeh M, Fedorova EE, Okamoto M, McLean E, Glass AD, Smith SE, Bisseling T, et al (2014) Soybean *SAT1* (*Symbiotic Ammonium Transporter 1*) encodes a bHLH transcription factor involved in nodule growth and NH_4^+ transport. Proc Natl Acad Sci USA **111:** 4814–4819

Coll NS, Epple P, Dangl JL (2011) Programmed cell death in the plant immune system. Cell Death Differ **18:** 1247–1256

Cosson V, Durand P, d'Erfurth I, Kondorosi A, Ratet P (2006) *Medicago truncatula* transformation using leaf explants. Methods Mol Biol **343:** 115–127

D'haeseleer K, De Keyser A, Goormachtig S, Holsters M (2010) Transcription factor MtATB2: About nodulation, sucrose and senescence. Plant Cell Physiol **51:** 1416–1424

de Zélicourt A, Diet A, Marion J, Laffont C, Ariel F, Moison M, Zahaf O, Crespi M, Gruber V, Frugier F (2012) Dual involvement of a *Medicago truncatula* NAC transcription factor in root abiotic stress response and symbiotic nodule senescence. Plant J **70:** 220–230

Dhanushkodi R, Matthew C, McManus MT, Dijkwel PP (2018) Drought-induced senescence of *Medicago truncatula* nodules involves serpin and ferritin to control proteolytic activity and iron levels. New Phytol **220:** 196–208

Domonkos Á, Kovács S, Gombár A, Kiss E, Horváth B, Kováts GZ, Farkas A, Tóth MT, Ayaydin F, Bóka K, et al (2017) NAD1 controls defense-like responses in *Medicago truncatula* symbiotic nitrogen fixing nodules Following rhizobial colonization in a bacA-independent manner. Genes (Basel) **8:** 387

Drewke C, Leistner E (2001) Biosynthesis of vitamin B6 and structurally related derivatives. Vitam Horm **61:** 121–155

Du JL, Zhang SW, Huang HW, Cai T, Li L, Chen S, He XJ (2015) The splicing factor PRP31 is involved in transcriptional gene silencing and stress response in *Arabidopsis*. Mol Plant **8:** 1053–1068

Duan M, Zhang R, Zhu F, Zhang Z, Gou L, Wen J, Dong J, Wang T (2017) A lipid-anchored NAC transcription factor is translocated into the nucleus and activates *Glyoxalase I* expression during drought stress. Plant Cell **29:** 1748–1772

Dupont L, Alloing G, Pierre O, El Msehli S, Hopkins J, Herouart D, Frendo P (2012) The legume root nodule: From symbiotic nitrogen fixation to senescence. In T Nagata, ed, Senescence. InTech, Rijeka, Croatia, pp 137–168

Fåhraeus G (1957) The infection of clover root hairs by nodule bacteria studied by a simple glass slide technique. J Gen Microbiol **16:** 374–381

Fedorova M, van de Mortel J, Matsumoto PA, Cho J, Town CD, VandenBosch KA, Gantt JS, Vance CP (2002) Genome-wide identification of nodule-specific transcripts in the model legume *Medicago truncatula*. Plant Physiol **130:** 519–537

Fox JE, Gulledge J, Engelhaupt E, Burow ME, McLachlan JA (2007) Pesticides reduce symbiotic efficiency of nitrogen-fixing rhizobia and host plants. Proc Natl Acad Sci USA **104:** 10282–10287

Fukudome M, Watanabe E, Osuki KI, Imaizumi R, Aoki T, Becana M, Uchiumi T (2019) Stably transformed *Lotus japonicus* plants overexpressing phytoglobin LjGlb1-1 show decreased nitric oxide levels in roots and nodules as well as delayed nodule senescence. Plant Cell Physiol **60:** 816–825

Godiard L, Lepage A, Moreau S, Laporte D, Verdenaud M, Timmers T, Gamas P (2011) MtbHLH1, a bHLH transcription factor involved in *Medicago truncatula* nodule vascular patterning and nodule to plant metabolic exchanges. New Phytol **191:** 391–404

Gómez LD, Baud S, Gilday A, Li Y, Graham IA (2006) Delayed embryo development in the *ARABIDOPSIS TREHALOSE-6-PHOSPHATE SYNTHASE 1* mutant is associated with altered cell wall structure, decreased cell division and starch accumulation. Plant J **46:** 69–84

González EM, Gálvez L, Arrese-Igor C (2001) Abscisic acid induces a decline in nitrogen fixation that involves leghaemoglobin, but is independent of sucrose synthase activity. J Exp Bot **52:** 285–293

Grudkowska M, Zagdańska B (2004) Multifunctional role of plant cysteine proteinases. Acta Biochim Pol **51:** 609–624

Guindon S, Dufayard JF, Lefort V, Anisimova M, Hordijk W, Gascuel O (2010) New algorithms and methods to estimate maximum-likelihood phylogenies: assessing the performance of PhyML 3.0. Syst Biol **59:** 307–321

Guinel FC (2015) Ethylene, a hormone at the center-stage of nodulation. Front Plant Sci **6:** 1121

Hädrich N, Hendriks JH, Kötting O, Arrivault S, Feil R, Zeeman SC, Gibon Y, Schulze WX, Stitt M, Lunn JE (2012) Mutagenesis of cysteine 81 prevents dimerization of the APS1 subunit of ADP-glucose pyrophosphorylase and alters diurnal starch turnover in *Arabidopsis thaliana* leaves. Plant J **70:** 231–242

Hakoyama T, Niimi K, Yamamoto T, Isobe S, Sato S, Nakamura Y, Tabata S, Kumagai H, Umehara Y, Brossuleit K, et al (2012) The integral membrane protein SEN1 is required for symbiotic nitrogen fixation in *Lotus japonicus* nodules. Plant Cell Physiol **53:** 225–236

Hayashi S, Gresshoff PM, Ferguson BJ (2014) Mechanistic action of gibberellins in legume nodulation. J Integr Plant Biol **56:** 971–978

Hedden P, Phillips AL (2000) Gibberellin metabolism: New insights revealed by the genes. Trends Plant Sci **5:** 523–530

Horváth B, Domonkos Á, Kereszt A, Szűcs A, Ábrahám E, Ayaydin F, Bóka K, Chen Y, Chen R, Murray JD, et al (2015) Loss of the nodule-specific cysteine rich peptide, NCR169, abolishes symbiotic nitrogen fixation in the *Medicago truncatula dnf7* mutant. Proc Natl Acad Sci USA **112:** 15232–15237

Kaiser BN, Finnegan PM, Tyerman SD, Whitehead LF, Bergersen FJ, Day DA, Udvardi MK (1998) Characterization of an ammonium transport protein from the peribacteroid membrane of soybean nodules. Science **281:** 1202–1206

Kardailsky IV, Brewin NJ (1996) Expression of cysteine protease genes in pea nodule development and senescence. Mol Plant Microbe Interact **9:** 689–695

Karmarkar V (2014) Transcriptional regulation of nodule development and senescence in Medicago truncatula. PhD thesis. Wageningen University, Wageningen, The Netherlands

Katoh K, Misawa K, Kuma K, Miyata T (2002) MAFFT: A novel method for rapid multiple sequence alignment based on fast Fourier transform. Nucleic Acids Res **30:** 3059–3066

Katoh K, Rozewicki J, Yamada KD (2017) MAFFT online service: Multiple sequence alignment, interactive sequence choice and visualization. Brief Bioinform **20:** 1160–1166

Kim M, Chen Y, Xi J, Waters C, Chen R, Wang D (2015) An antimicrobial peptide essential for bacterial survival in the nitrogen-fixing symbiosis. Proc Natl Acad Sci USA **112:** 15238–15243

Krusell L, Krause K, Ott T, Desbrosses G, Krämer U, Sato S, Nakamura Y, Tabata S, James EK, Sandal N, et al (2005) The sulfate transporter SST1 is crucial for symbiotic nitrogen fixation in *Lotus japonicus* root nodules. Plant Cell **17:** 1625–1636

Kumagai H, Hakoyama T, Umehara Y, Sato S, Kaneko T, Tabata S, Kouchi H (2007) A novel ankyrin-repeat membrane protein, IGN1, is required for persistence of nitrogen-fixing symbiosis in root nodules of *Lotus japonicus*. Plant Physiol **143:** 1293–1305

Larkin MA, Blackshields G, Brown NP, Chenna R, McGettigan PA, McWilliam H, Valentin F, Wallace IM, Wilm A, Lopez R, et al (2007) Clustal W and clustal X version 2.0. Bioinformatics **23:** 2947–2948

Li Q, Lau A, Morris TJ, Guo L, Fordyce CB, Stanley EF (2004) A syntaxin 1, Galpha(o), and N-type calcium channel complex at a presynaptic nerve terminal: Analysis by quantitative immunocolocalization. J Neurosci **24:** 4070–4081

Li X, Feng H, Wen J, Dong J, Wang T (2018) MtCAS31 aids symbiotic nitrogen fixation by protecting the leghemoglobin MtLb120-1 under drought stress in *Medicago truncatula*. Front Plant Sci **9:** 633

Li Y, Zhou L, Li Y, Chen D, Tan X, Lei L, Zhou J (2008) A nodule-specific plant cysteine proteinase, AsNODF32, is involved in nodule senescence and nitrogen fixation activity of the green manure legume *Astragalus sinicus*. New Phytol **180:** 185–192

Lohman KN, Gan S, John MC, Amasino RM (1994) Molecular analysis of natural leaf senescence in *Arabidopsis thaliana*. Physiol Plant **92:** 322–328

Ma L, Zhu F, Li Z, Zhang J, Li X, Dong J, Wang T (2015) TALEN-based mutagenesis of lipoxygenase LOX3 enhances the storage tolerance of rice (*Oryza sativa*) seeds. PLoS One **10:** e0143877

Mao X, Cai T, Olyarchuk JG, Wei L (2005) Automated genome annotation and pathway identification using the KEGG Orthology (KO) as a controlled vocabulary. Bioinformatics **21:** 3787–3793

Marini AM, Springael JY, Frommer WB, André B (2000) Cross-talk between ammonium transporters in yeast and interference by the soybean SAT1 protein. Mol Microbiol **35:** 378–385

Naito Y, Fujie M, Usami S, Murooka Y, Yamada T (2000) The involvement of a cysteine proteinase in the nodule development in Chinese milk vetch infected with *Mesorhizobium huakuii* subsp. *rengei*. Plant Physiol **124:** 1087–1096

Navascués J, Pérez-Rontomé C, Gay M, Marcos M, Yang F, Walker FA, Desbois A, Abián J, Becana M (2012) Leghemoglobin green derivatives with nitrated hemes evidence production of highly reactive nitrogen species during aging of legume nodules. Proc Natl Acad Sci USA **109:** 2660–2665

Oh CJ, Lee H, Kim H, An CS (2004) Isolation and characterization of a root nodule-specific cysteine proteinase cDNA from soybean. J Plant Biol **47:** 216–220

Okamoto T (2006) Transport of proteases to the vacuole: ER export bypassing Golgi? In DG Robinson, ed, The Plant Endoplasmic Reticulum. Springer-Verlag, Heidelberg, Germany, pp 125–139

Pérez Guerra JC, Coussens G, De Keyser A, De Rycke R, De Bodt S, Van De Velde W, Goormachtig S, Holsters M (2010) Comparison of developmental and stress-induced nodule senescence in *Medicago truncatula*. Plant Physiol **152:** 1574–1584

Pierre O, Hopkins J, Combier M, Baldacci F, Engler G, Brouquisse R, Hérouart D, Boncompagni E (2014) Involvement of papain and legumain proteinase in the senescence process of *Medicago truncatula* nodules. New Phytol **202:** 849–863

Pladys D, Vance CP (1993) Proteolysis during development and senescence of effective and plant gene-controlled ineffective alfalfa nodules. Plant Physiol **103:** 379–384

Plet J, Wasson A, Ariel F, Le Signor C, Baker D, Mathesius U, Crespi M, Frugier F (2011) MtCRE1-dependent cytokinin signaling integrates bacterial and plant cues to coordinate symbiotic nodule organogenesis in *Medicago truncatula*. Plant J **65:** 622–633

Puppo A, Groten K, Bastian F, Carzaniga R, Soussi M, Lucas MM, de Felipe MR, Harrison J, Vanacker H, Foyer CH (2005) Legume nodule senescence: Roles for redox and hormone signalling in the orchestration of the natural aging process. New Phytol **165:** 683–701

Richau KH, Kaschani F, Verdoes M, Pansuriya TC, Niessen S, Stüber K, Colby T, Overkleeft HS, Bogyo M, Van der Hoorn RA (2012) Subclassification and biochemical analysis of plant papain-like cysteine proteases displays subfamily-specific characteristics. Plant Physiol **158:** 1583–1599

Roux B, Rodde N, Jardinaud MF, Timmers T, Sauviac L, Cottret L, Carrère S, Sallet E, Courcelle E, Moreau S, et al (2014) An integrated analysis of plant and bacterial gene expression in symbiotic root nodules using laser-capture microdissection coupled to RNA sequencing. Plant J **77:** 817–837

Saleh A, Alvarez-Venegas R, Avramova Z (2008) An efficient chromatin immunoprecipitation (ChIP) protocol for studying histone modifications in *Arabidopsis* plants. Nat Protoc **3:** 1018–1025

Serova TA, Tikhonovich IA, Tsyganov VE (2017) Analysis of nodule senescence in pea (*Pisum sativum* L.) using laser microdissection, real-time PCR, and ACC immunolocalization. J Plant Physiol **212:** 29–44

Serova TA, Tsyganova AV, Tikhonovich IA, Tsyganov VE (2019) Gibberellins inhibit nodule senescence and stimulate nodule meristem bifurcation in pea (*Pisum sativum* L.). Front Plant Sci **10:** 285

Shan W, Kuang JF, Chen L, Xie H, Peng HH, Xiao YY, Li XP, Chen WX, He QG, Chen JY, et al (2012) Molecular characterization of banana NAC transcription factors and their interactions with ethylene signalling component EIL during fruit ripening. J Exp Bot **63:** 5171–5187

Sheokand S, Dahiya P, Vincent JL, Brewin NJ (2005) Modified expression of cysteine protease affects seed germination, vegetative growth and nodule development in transgenic lines of *Medicago truncatula*. Plant Sci **169:** 966–975

ShuoHao H, Jing L, Jie Z, JianYun Z, LongQuan H (2019) Identification and characterization of a pyridoxal 5′-phosphate phosphatase in tobacco plants. Plant Sci **278:** 88–95

Sinharoy S, Torres-Jerez I, Bandyopadhyay K, Kereszt A, Pislariu CI, Nakashima J, Benedito VA, Kondorosi E, Udvardi MK (2013) The C_2H_2 transcription factor regulator of symbiosome differentiation represses transcription of the secretory pathway gene *VAMP721a* and promotes symbiosome development in *Medicago truncatula*. Plant Cell **25:** 3584–3601

Stonoha-Arther C, Wang D (2018) Tough love: Accommodating intracellular bacteria through directed secretion of antimicrobial peptides during the nitrogen-fixing symbiosis. Curr Opin Plant Biol **44:** 155–163

Sun TP (2008) Gibberellin metabolism, perception and signaling pathways in Arabidopsis. Arabidopsis Book **6:** e0103

Tao Q, Guo D, Wei B, Zhang F, Pang C, Jiang H, Zhang J, Wei T, Gu H, Qu LJ, et al (2013) The TIE1 transcriptional repressor links TCP transcription factors with TOPLESS/TOPLESS-RELATED corepressors and modulates leaf development in *Arabidopsis*. Plant Cell **25:** 421–437

Timmers AC, Soupène E, Auriac MC, de Billy F, Vasse J, Boistard P, Truchet G (2000) Saprophytic intracellular rhizobia in alfalfa nodules. Mol Plant Microbe Interact **13:** 1204–1213

Trujillo DI, Silverstein KAT, Young ND (2019) Nodule-specific PLAT domain proteins are expanded in the *Medicago* lineage and required for nodulation. New Phytol **222:** 1538–1550

Tse YC, Lo SW, Hillmer S, Dupree P, Jiang L (2006) Dynamic response of prevacuolar compartments to brefeldin a in plant cells. Plant Physiol **142:** 1442–1459

Van de Velde W, Guerra JC, De Keyser A, De Rycke R, Rombauts S, Maunoury N, Mergaert P, Kondorosi E, Holsters M, Goormachtig S (2006) Aging in legume symbiosis. A molecular view on nodule senescence in *Medicago truncatula*. Plant Physiol **141:** 711–720

van der Hoorn RA (2008) Plant proteases: From phenotypes to molecular mechanisms. Annu Rev Plant Biol **59:** 191–223

Vandesompele J, De Preter K, Pattyn F, Poppe B, Van Roy N, De Paepe A, Speleman F (2002) Accurate normalization of real-time quantitative RT-PCR data by geometric averaging of multiple internal control genes. Genome Biol **3:** RESEARCH0034

Vincent JL, Brewin NJ (2000) Immunolocalization of a cysteine protease in vacuoles, vesicles, and symbiosomes of pea nodule cells. Plant Physiol **123:** 521–530

Wang C, Yu H, Luo L, Duan L, Cai L, He X, Wen J, Mysore KS, Li G, Xiao A, et al (2016) *NODULES WITH ACTIVATED DEFENSE 1* is required for maintenance of rhizobial endosymbiosis in *Medicago truncatula*. New Phytol **212:** 176–191

Wang Q, Liu J, Li H, Yang S, Körmöczi P, Kereszt A, Zhu H (2018) Nodule-specific cysteine-rich peptides negatively regulate nitrogen-fixing symbiosis in a strain-specific manner in *Medicago truncatula*. Mol Plant Microbe Interact **31:** 240–248

Wang Q, Yang S, Liu J, Terecskei K, Ábrahám E, Gombár A, Domonkos Á, Szűcs A, Körmöczi P, Wang T, et al (2017) Host-secreted antimicrobial peptide enforces symbiotic selectivity in *Medicago truncatula*. Proc Natl Acad Sci USA **114:** 6854–6859

Xi J, Chen Y, Nakashima J, Wang SM, Chen R (2013) *Medicago truncatula esn1* defines a genetic locus involved in nodule senescence and symbiotic nitrogen fixation. Mol Plant Microbe Interact **26:** 893–902

Xiang L, Etxeberria E, Van den Ende W (2013) Vacuolar protein sorting mechanisms in plants. FEBS J **280:** 979–993

Xing HL, Dong L, Wang ZP, Zhang HY, Han CY, Liu B, Wang XC, Chen QJ (2014) A CRISPR/Cas9 toolkit for multiplex genome editing in plants. BMC Plant Biol **14:** 327

Yamaya-Ito H, Shimoda Y, Hakoyama T, Sato S, Kaneko T, Hossain MS, Shibata S, Kawaguchi M, Hayashi M, Kouchi H, et al (2018) Loss-of-function of ASPARTIC PEPTIDASE NODULE-INDUCED 1 (APN1) in *Lotus japonicus* restricts efficient nitrogen-fixing symbiosis with specific *Mesorhizobium loti* strains. Plant J **93:** 5–16

Yang S, Wang Q, Fedorova E, Liu J, Qin Q, Zheng Q, Price PA, Pan H, Wang D, Griffitts JS, et al (2017) Microsymbiont discrimination mediated by a host-secreted peptide in *Medicago truncatula*. Proc Natl Acad Sci USA **114:** 6848–6853

Young MD, Wakefield MJ, Smyth GK, Oshlack A (2010) Gene ontology analysis for RNA-seq: Accounting for selection bias. Genome Biol **11:** R14

Young ND, Debellé F, Oldroyd GE, Geurts R, Cannon SB, Udvardi MK, Benedito VA, Mayer KF, Gouzy J, Schoof H, et al (2011) The *Medicago* genome provides insight into the evolution of rhizobial symbioses. Nature **480:** 520–524

Zhang H, Cui F, Wu Y, Lou L, Liu L, Tian M, Ning Y, Shu K, Tang S, Xie Q (2015) The RING finger ubiquitin E3 ligase SDIR1 targets

SDIR1-INTERACTING PROTEIN1 for degradation to modulate the salt stress response and ABA signaling in *Arabidopsis*. Plant Cell **27:** 214–227

Zhang H, Gao S, Lercher MJ, Hu S, Chen WH (2012a) EvolView, an online tool for visualizing, annotating and managing phylogenetic trees. Nucleic Acids Res **40:** W569–W572

Zhang K, Xia X, Zhang Y, Gan SS (2012b) An ABA-regulated and Golgi-localized protein phosphatase controls water loss during leaf senescence in *Arabidopsis*. Plant J **69:** 667–678

Zhang Z, Hu X, Zhang Y, Miao Z, Xie C, Meng X, Deng J, Wen J, Mysore KS, Frugier F, et al (2016) Opposing control by transcription factors MYB61 and MYB3 increases freezing tolerance by relieving C-repeat binding factor suppression. Plant Physiol **172:** 1306–1323

Zhou J, Lu D, Xu G, Finlayson SA, He P, Shan L (2015) The dominant negative ARM domain uncovers multiple functions of PUB13 in Arabidopsis immunity, flowering, and senescence. J Exp Bot **66:** 3353–3366